Title: Serotonergic modulation of visual neurons in *Drosophila melanogaster*

Abbreviated Title: Serotonergic modulation of visual neurons in *Drosophila*

Authors: Maureen M Sampson[1,2]*, Katherine M Myers Gschweng[1,3]*, Ben J Hardcastle[4], Shivan L Bonanno[1,3], Tyler R Sizemore[5], Rebecca C Arnold[1,3], Fuying Gao[3], Andrew M Dacks[5], Mark A Frye[4], David E Krantz[1,3]

*These authors contributed equally

[1]UCLA, Hatos Center for Neuropharmacology, Los Angeles, CA, USA, 90095

[2]UCLA, Molecular Toxicology Interdepartmental Program, Los Angeles, CA, USA, 90095

[3]UCLA, Psychiatry and Biobehavioral Sciences, David Geffen School of Medicine, Los Angeles, CA, USA, 90095

[4]UCLA, Department of Integrative Biology and Physiology, Los Angeles, CA, USA, 90095

[5]Department of Biology, West Virginia University, Morgantown, WV, USA, 26506

Correspondence should be addressed to David Krantz at dkrantz@ucla.edu or
3357C GONDA CENTER FOR NEUROSCIENCE AND GENETICS
695 CHARLES YOUNG DR, SO.LOS ANGELES, CA 90095-1761 USA

No. Pages: 58

No. Figures: 8

No. Words in Abstract: 235/250

No. Words in Intro: 613/650

No. Words in Discussion: 1506/1500

Acknowledgements: We thank members of Larry Zipursky's lab (UCLA) including Elizabeth Zuniga Sanchez, Liming Tan, and Juyoun Yoo for advice on FACS, RNA extraction, RT-qPCR and SMART-Seq. Thank you to Aditya Eamani (UCLA), Deanne Umbay (Brown University) and Nikoo Dalili (UCLA) for their assistance in the lab. We

thank all other members of the Frye and Krantz labs for helpful discussions, and Aljoscha Nern (HHMI/Janelia Research Campus), Herman Dierick (Baylor), and Yi Rao (Peking University) for generously supplying fly lines.

Conflict of Interest: The authors deny any relevant paid employment or consultancy, stock ownership, patent applications, personal relationships with relevant individuals, or membership of an advisory board.

Abstract

Sensory systems rely on neuromodulators, such as serotonin, to provide flexibility in the face of a highly variable stimulus space, and serotonin modulates a variety of circuits in both mammals and invertebrates. Serotonergic neurons innervate the optic ganglia of *Drosophila melanoaster*, a widely used model for the study of visual behavior. However, the functional role of serotonin in *Drosophila* vision is not known. To address this question, we mapped serotonin receptor expression in the first optic ganglion, the lamina, and tested whether serotonin regulates the physiology of a subset of laminar neurons. Serotonin receptors are expressed in multiple lamina cells including 5-HT2B in laminar monopolar cell L2, required for the initial steps of visual processing, and both 5-HT1A and 5-HT1B in T1 cells, whose function in vision is unknown. Subcellular mapping with GFP-tagged receptors showed that 5-HT2B in L2 and 5-HT1A in T1 localize to the nerve terminals, suggesting that the medulla is the primary site of serotonergic regulation for these neurons. Indeed, serotonin increases intracellular calcium in L2 nerve terminals, and this response was ablated by mutation of 5-HT2B. Serotonin also alters the kinetics of visually induced calcium transients in L2 following dark flashes, and this too was ablated by loss of 5-HT2B. Our study demonstrates that a subset of neurons involved in the initial steps of visual processing are regulated by serotonin and establishes a new platform for the study of serotonergic neuromodulation.

Significance Statement

58 Serotonin signaling is mediated by complex array of receptor subtypes. The
59 molecular mechanisms by which these receptors regulate circuit activity and behavior
60 remain unclear. The visual system of *Drosophila* offers a potential genetic model to
61 study serotonin neuromodulation, yet previous studies have not determined how
62 serotonin modulates the function of neurons in the visual system, nor demonstrated the
63 contribution of specific serotonin receptors. We provide the first functional data showing
64 a role for specific serotonin receptors in neurons required for initiating visual processing
65 in *Drosophila*. Our data establish a new model for studying the mechanisms by which
66 serotonin regulate vision and related behaviors.

67

68 **Introduction**

69 Serotonin acts a neuromodulator (Marder, 2012, Marder et al., 2014, Nadim and
70 Bucher, 2014) in a variety of networks including the sensory systems required for
71 olfaction and vision (e.g. (Dacks et al., 2008, Petzold et al., 2009, Brunert et al., 2016,
72 Lottem et al., 2016, Seillier et al., 2017)). In the mammalian visual cortex, serotonin
73 regulates the balance of excitation and inhibition (Moreau et al., 2010), cellular plasticity
74 (Gagolewicz and Dringenberg, 2016, Lombaert et al., 2018), and response gain (Seillier
75 et al., 2017). In some cases, the contribution of individual receptor subtypes is known;
76 for example, in the mammalian retina, serotonin signaling reduces GABAergic amacrine
77 cell input to retinal ganglion cells (RGCs) via 5-HT1A (Zhou et al., 2018) and can
78 modulate the response of RGCs to visual stimuli (Trakhtenberg et al., 2017). However,
79 for most sensory circuits, the manner in which serotonin receptor activation regulates
80 information processing remains poorly understood.

81 The visual system of *Drosophila melanogaster* provides a powerful genetic model
82 to study visual circuits as well as their regulation (Borst and Helmstaedter, 2015, Cheng
83 and Frye, 2019). In *Drosophila,* visual processing begins in the lamina where intrinsic
84 monopolar neurons receive direct input from photoreceptors (Meinertzhagen and O'Neil,
85 1991). Lamina monopolar cells L1 and L2 respond to changes in luminance and signal
86 to downstream medulla neurons (Joesch et al., 2010, Strother et al., 2014, Yang et al.,
87 2016). Significant progress has been made in mapping the synaptic connectivity and
88 function of visual processing neurons, including those required for motion detection
89 (Meinertzhagen and O'Neil, 1991, Takemura et al., 2008, Rivera-Alba et al., 2011,
90 Takemura et al., 2017a, Shinomiya et al., 2019). Additional studies have uncovered
91 some neuromodulatory pathways that regulate visual processing neurons (Cheng and
92 Frye, 2019). However, our understanding of neuromodulatory processes in the visual
93 system lag far behind the more extensive study of synaptic connectivity and behavior
94 (Borst and Helmstaedter, 2015, Sanes and Zipursky, 2010).

95 Serotonergic neurons broadly innervate the *Drosophila* optic ganglia (Nässel,
96 1988, Valles and White, 1988) and previous studies indicate that serotonin may impact
97 cellular activity and visual behavior in insects. In the blowfly, serotonin altered
98 electrophysiological field recordings representing the combined output of L1 and L2
99 neurons (Chen et al., 1999). In the honeybee, single cell recordings in motion-sensitive
100 lobula neurons showed that serotonin signaling reduces directional selectivity and
101 amplitude of field potentials evoked by moving stripes (Kloppenburg and Erber, 1995).
102 In the house fly, serotonin regulates rhythmic size changes in L1 and L2 terminals in the
103 medulla (Pyza and Meinertzhagen, 1996) and in *Drosophila*, serotonin modulates the

104 voltage dependence of potassium channels in photoreceptors (Hevers and Hardie,
105 1995). To date, the molecular mechanisms responsible for these effects and the
106 potential contributions of specific subtypes of serotonin receptors to the functions of the
107 fly visual system remains unknown.

108 The cellular effects of serotonin signaling are highly complex due to diverse
109 secondary messenger cascades (Nichols and Nichols, 2008, McCorvy and Roth, 2015)
110 and combinatorial expression of receptors within a single cell (Araneda and Andrade,
111 1991, Maroteaux et al., 2019) or circuit (Celada et al., 2013). Moreover, receptors can
112 induce both immediate and long-term changes in physiology. The precise effect of
113 serotonin receptor activation in specific cells are difficult to predict and necessitates the
114 use of functional assays to complement expression studies. Although one other study
115 has recently reported serotonin receptor expression in visual neurons (Davis et al.,
116 2020), to our knowledge there is no information on the functional effect(s) of any
117 serotonin receptor in any cell within the fly visual system. In this work, we show how a
118 specific serotonin receptor, 5-HT2B, regulates visual processing in one of the lamina
119 neurons, L2, responsible for the initiation of visual processing.

120

121 **Methods**

122 **Fly Husbandry and Genetic Lines**

123 Flies were maintained on a standard cornmeal and molasses-based agar media
124 with a 12:12 hour light/dark cycle at room temperature (22-25°C). Serotonin receptor
125 MiMIC-T2A-GAL4 lines described in (Gnerer et al., 2015) were a gift from Herman

126 Dierick (Baylor College of Medicine), and include 5-HT1A-GAL4^{MI01468}, 5-HT1A-
127 GAL4^{MI01140}, 5-HT1A-T2A-GAL4^{MI04464}, 5-HT1B-T2A-GAL4^{MI05213}, 5-HT2A-GAL4 ^{MI0459},
128 5-HT2A-GAL4 ^{MI03299}, 5-HT2B-T2A-GAL4^{MI06500}, 5-HT2B-T2A-GAL4^{MI5208}, 5-HT2B-
129 GAL4^{MI7403}, and 5-HT7GAL4 ^{MI00215}. Split-GAL4 and LexA lines for L1 and T1 (Tuthill et
130 al., 2013) were provided by Aljoscha Nern (HHMI/Janelia Research Campus). L.
131 Zipursky generously provided L2-split-GAL4 and L2-LexA (RRID:BDSC_52510). Yi Rao
132 (Peking University) generously shared 5-HT2B GAL4 SII (5-HT2B mutant) (Qian et al.,
133 2017), 5-HT1A::sfGFP (Deng et al., 2019), and UAS-5-HT2B::sfGFP (Qian et al., 2017).

134 Reporter lines include: UAS-mCD8::GFP (RRID:BDSC_5137), UAS-MCFO-1
135 (RRID:BDSC_64085), UAS-GCaMP6f (RRID:BDSC_42747), UAS-ArcLight
136 (RRID:BDSC_51056), UAS-DenMark, UAS-Syt.eGFP (RRID:BDSC_33064 and
137 RRID:BDSC_33065), UAS-mCD8::RFP, LexAop-mCD8::GFP (RRID:BDSC_32229),
138 and UAS-nSyb::GFP1-10, LexAop-CD4:GFP11 (RRID:BDSC_64314; provided by Larry
139 Zipursky (UCLA)).

140

141 **Immunohistochemistry**

142 Flies were dissected 5-10 days after eclosion, and equal numbers of males and
143 females were used for all experiments unless otherwise noted. Brains were dissected in
144 ice-cold PBS (Alfa Aesar, Cat#J62036, Tewksbury, MA), then fixed in 4%
145 paraformaldehyde (FisherScientific, Cat#50-980-493, Waltham, MA) in PBS with 0.3%
146 Triton X-100 (Millipore Sigma, Cat#X100, Burlington, MA) (PBST) for one hour at room
147 temperature. After fixation, brains were washed three times with PBST for 10 minutes,

148 then blocked for 30 minutes in PBST containing 0.5% normal goat serum (NGS)
149 (Cayman Chemical, Cat#10006577, Ann Arbor, MA) PBST. Antibodies were diluted in
150 0.5% NGS/PBST. Primary antibodies were incubated with the tissue overnight at 4°C.
151 The next day, the brains were washed three times with PBST for 10 minutes, then
152 incubated with secondary antibodies for 2 hours in the dark at room temperature. Brains
153 were washed three times with PBST for 10 minutes before mounting.

154 For frontal mounting, brains were washed with 60% and 80% glycerol (Millipore
155 Sigma, Cat#G5516) and mounted in Fluoromount-G (SouthernBiotech, Cat#0100-01,
156 Birmingham, AL). For dorsal-ventral mounting, brains were fixed in 2% PFA/PBST
157 overnight. The next day, brains were washed three times with PBST. Brains were
158 dehydrated with a series of 10 min ethanol baths of increasing concentrations (30%,
159 50%, 75%, 95%, 100%, 100%, and 100%). Brains were then transferred to 100%
160 xylene before mounting in DPX (FisherScientific, Cat#50-980-370).

161 Serotonin immunolabeling was performed with 1:25 rat anti-serotonin (Millipore
162 Sigma, Cat#MAB352, RRID:AB_11213564), 1:1000 rabbit anti-serotonin (ImmunoStar,
163 Cat#20080, Hudson, WI ,RRID:AB_572263) or 1:1000 goat anti-serotonin (ImmunoStar,
164 Cat#20079, RRID:AB_572262). GFP was labeled with 1:250 mouse anti-GFP (Sigma-
165 Aldrich, Cat#G6539, RRID:AB_259941; or, ThermoFisher, Waltham, MA, Cat#A-11120,
166 RRID:AB_221568). Secondary antibodies were used at 1:400 and include: Alexa Fluor
167 488, 594 or 647 (Jackson ImmunoResearch Laboratories, Westgrove, PA, Cat#715-
168 545-151, # 711-585-152, # 712-605-153) or Alexa Fluor 555 (Life Technologies,
169 ThermoFisher, Cat#A-21428).

170 MultiColor FlpOut (MCFO-1) sparse labeling was induced by heat activation at
171 37°C for 10-15 minutes at least 2 days prior to dissection as described (Nern et al.,
172 2015). Primary antibodies included 1:300 rabbit anti-HA (Cell Signaling Technology,
173 Cat#3724, Danvers, MA, RRID:AB_1549585), 1:150 rat anti-FLAG (Novus, Littleton,
174 CA, Cat#NBP1-06712, RRID:AB_1625982), and 1:400 anti-V5::Dylight-550 (Bio-Rad,
175 Hercules, CA, Cat#MCA1360D550GA, RRID:AB_2687576).

176

177 **Imaging and Image Processing**

178 Imaging was performed with a Zeiss LSM 880 Confocal with Airyscan (Zeiss,
179 Oberkochen, Germany) using a 40x water or 63x oil immersion objective. Post-hoc
180 processing of images was done with Fiji (Schindelin et al., 2012) or Adobe Photoshop
181 (Adobe, San Jose, CA) . All adjustments were applied to every pixel in the image. In
182 some cases we applied non-linear adjustments across the entire image.

183

184 **FACS and RNA Extraction**

185 L2, T1 and L1 neurons were labeled using split-GAL4 drivers (Tuthill et al., 2013)
186 combined with UAS-mCD8::GFP (RRID:BDSC_5137). Brains were dissected on the
187 day of eclosion and optic lobes were dissociated according to previously published
188 methods (Tan et al., 2015). The dissociated optic lobe cells were separated by
189 fluorescence-activated cell sorting (FACS) into GFP-positive and GFP-negative isolates
190 using a BD FACS Aria II high-speed cell sorter. Flow cytometry was performed in the
191 UCLA Jonsson Comprehensive Cancer Center (JCCC) and Center for AIDS Research

192 Flow Cytometry Core Facility that is supported by National Institutes of Health awards
193 P30 CA016042 and 5P30 AI028697, and by the JCCC, the UCLA AIDS Institute, the
194 David Geffen School of Medicine at UCLA, the UCLA Chancellor's Office, and the UCLA
195 Vice Chancellor's Office of Research. For FACS, each experiment was performed with
196 18-40 brains, and yielded between 1,700-7,800 GFP^+ cells. RNA was extracted from
197 isolated cells with ARCTURUS® PicoPure® RNA Isolation Kit (ThermoFisher, KIT0204)
198 or RNeasy Plus Micro Kit (QIAGEN, 74034).

199

200 **RT-qPCR**

201 RNA extracted from FACS isolates was reverse transcribed using SuperScript III
202 (Invitrogen, ThermoFisher, Cat#18080093). RT-qPCR was performed for receptor
203 cDNA using validated primers (Table 1) and SYBR Green Power PCR Mix (Applied
204 Biosystems, ThermoFisher) on an iQ5 real-time qPCR detection system (Bio-Rad).
205 Primers were designed using Primer-Blast (https://www.ncbi.nlm.nih.gov/tools/primer-
206 blast/) or were from the DGRC FlyPrimerBank (Hu et al., 2013); oligonucleotides were
207 obtained from Integrated DNA Technologies (Coralville, Iowa). Primer pairs were
208 validated to amplify a single product, verified by a single melting temperature and single
209 band on an electrophoresis gel. The efficiency for each primer pair was between 85-
210 115%. Comparisons between GFP^+ and GFP^- samples were calculated as enrichment
211 (i.e., fold change) using the comparative CT method (Schmittgen and Livak, 2008). A
212 zero value was imputed for samples with no amplification (i.e., no CT value).

213

214 **Table 1.** RT-qPCR primer sequences and mRNA (cDNA) target information.

S1 Table. Primer sequences and mRNA target information.

Primer ID	Gene Symbol	Primer Sequence (5' to 3')	Transcript Specificity	Design
5HT1A Forward	Dmel\5-HT1A	TTCGTGGCCTGCCTAGTAAT	All	BLAST
5HT1A Reverse	Dmel\5-HT1A	CCAGTAACGATCGACGGCAA	All	BLAST
5HT2B Forward	Dmel\5-HT2B	AAAGCCGATTGCTTCTCCAAC	All	BLAST
5HT2B Reverse	Dmel\5-HT2B	GATTCAGGACTCGCGAAAGG	All	BLAST
5HT1B Forward	Dmel\5-HT1B	ATTTCGCCAGTTTGGCCATT	All	BLAST
5HT1B Reverse	Dmel\5-HT1B	CGTTGCTGGTGCGATAATCA	All	BLAST
5HT7 Forward	Dmel\5-HT7	TCGACGACTTTTGGAAGCAC	All	BLAST
5HT7 Reverse	Dmel\5-HT7	ATTGTCGTCGGGAACTGGG	All	BLAST
5HT2A Forward	Dmel\5-HT2A	CGACTGCAAAATGTGGGTCT	All except F	BLAST
5HT2A Reverse	Dmel\5-HT2A	CCTCGCAGATGTGTCTGTTG	All except F	BLAST
RP49 Forward	Dmel\RpL32	GGTTTCCGGCAAGCTTCAA	B Only	BLAST
RP499 Reverse	Dmel\RpL32	TGTTGTCGATACCCTTGGGC	B Ony	BLAST
PP3447 Forward	Dmel\shakB	ACACCAAGATGGCTGTGGAAA	All	DGRC
PP3447 Reverse	Dmel\shakB	GCTTCGGAACAAATGCCTATGTC	All	DGRC

215

216

217 **RNA-Seq**

218 RNA-Seq was performed using a SMART-Seq protocol adapted from (Picelli et
219 al., 2013, Picelli et al., 2014, Tan et al., 2015). Libraries were constructed using the
220 SMART-seq v4 Ultra Low-input RNA sequencing kit with Nextera XT (Takara Bio).
221 Paired-end sequencing was conducted by the UCLA genomic core facility
222 (https://www.semel.ucla.edu/ungc/services). After demultiplexing, we obtained between
223 39-270 (average 105) million reads per sample. Quality control was performed on base

224 qualities and nucleotide composition of sequences. Alignment to the *Drosophila*
225 *melanogaster* genome (BDGP6) was performed using the STAR spliced read aligner
226 (Dobin et al., 2013) with default parameters. Additional QC was performed after the
227 alignment to examine the following: level of mismatch rate, mapping rate to the whole
228 genome, repeats, chromosomes, and key transcriptomic regions (exons, introns, UTRs,
229 genes). Between 75-85% of the reads mapped uniquely to the fly genome. Total counts
230 of read fragments aligned to candidate gene regions within the reference gene
231 annotation were derived using HTSeq program and used as a basis for the
232 quantification of gene expression. Only uniquely mapped reads were used for
233 subsequent analyses. Following alignment and read quantification, we performed
234 quality control using a variety of indices, including consistency of replicates and average
235 gene coverage. For Fig 4D, L2 samples were run in two separate sequencing runs and
236 we did not perform corrections for any potential batch effects. Data is shown as
237 Transcripts Per Million (TPMs).

238

239 **Live Cell Imaging**

240 Calcium imaging was performed as previously described (Keles and Frye, 2017).
241 Briefly, flies were anesthetized at 4°C and placed into a chemically etched metal shim
242 within a larger custom-built fly holder. The fly holder was based on a previously
243 described design (Weir and Dickinson, 2015). The head capsule and the thorax were
244 glued to the metal shim using UV-curable glue (www.esslinger.com). The legs,
245 proboscis and antennae were immobilized using beeswax applied with a heated metal
246 probe (Waxelectric-1, Renfert). The head capsule was immersed in insect saline (103

247 mM NaCl, 3 mM KCl, 1.5mM CaCl2, 4 mM MgCl2, 26 mM NaHCO3, 1 mM NaH2PO4,
248 10 mM trehalose, 10 mM glucose, 5 mM TES, 2 mM sucrose) (Wilson et al., 2004). A
249 small window on the right rear head capsule was opened using sharp forceps (Dumont,
250 #5SF). Muscles and fat covering the optic lobe were cleared before placing the fly under
251 the 2-photon microscope (VIVO, 3i: Intelligent Imaging Innovations, Denver, CO).
252 Neurons expressing GCaMP6f were imaged at 920-nm using a Ti:Sapphire Laser
253 (Chameleon Vision, Coherent). Images were acquired at 10-20 frames/s. Only female
254 flies were used for live imaging experiments.

255 A custom-built gravity perfusion system was used for bath application of either
256 serotonin or saline control to the fly's exposed optic lobe. For Fig 6, the tissue was first
257 perfused with insect saline containing 1μm tetrodotoxin citrate (TTX) (Alomone Labs,
258 Jerusalem, Israel, Cat#T-550) for at least 5 minutes at 2 mL/min, prior to each
259 recording. TTX remained present throughout the experiment. To examine the effects of
260 serotonin on calcium levels, baseline GCaMP6f fluorescence was recorded for one
261 minute before switching to the second input containing either 100μM serotonin
262 hydrochloride (Sigma Aldrich, Cat# H9523) or saline alone for an additional five minutes
263 of recording. Due to perfusion tubing length and dead volume, the perfusion switch took
264 approximately 1 min 45 s to reach the tissue.

265

266 **Visual Stimulus Experiments**

267 Visual stimuli were shown using an arena composed of 48 eight by eight-pixel
268 LED panels, at 470 nm (Adafruit, NY, NY). The panels were assembled into a curved

269 display that extends 216° along the azimuth and ±35° in elevation. Each pixel
270 subtended an angle of 2.2° on the retina at the equatorial axis. To prevent spurious
271 excitation of the imaging photomultiplier tubes, three layers of blue filter (Rosco no. 59
272 Indigo) were placed over the LED display.

273 Each stimulus consisted of a brief increment (light flash) or decrement (dark
274 flash) of the entire display for 100 ms, before returning to a mid-intensity brightness for
275 4.9 s. Images were acquired at 25-30 frames/s. Stimuli were presented in sets of six
276 bright and six dark flashes randomly shuffled for each minute of the experiment.
277 Responses were then pooled for each minute. During the first minute, and prior to
278 imaging, the tissue was perfused with saline for a baseline recording. At the end of the
279 first minute, a valve controller (VC-6, Warner Instruments, Hamden, CT) activated by a
280 TTL signal switched the perfusion to either saline with 100 μM serotonin or saline alone;
281 imaging then continued for an additional five minutes, for a total of one baseline set and
282 five post-switch sets of stimuli. The perfusion switch took approximately 45 s to reach
283 the tissue.

284

285 **Live Imaging Analysis**

286 Calcium imaging data were analyzed with Matlab R2017a (Mathworks, Natick,
287 MA). Post hoc, recordings were corrected for movement of the brain within the imaging
288 plane using a custom algorithm (Akin and Zipursky, 2016). Regions of interest (ROIs)
289 were found semi-automatically for data in Figs 6-8: first, the median intensity of all pixels
290 across all image frames was found; this value was used as a threshold and all pixels

291 with mean intensity below the threshold, typically within the image background, were
292 discarded. The 1-D time series of intensity for each remaining pixel was then extracted.
293 K-means clustering was used to identify pixels with similar activity over the course of the
294 experiment: three clusters were identified and the cluster with the highest number of
295 pixels was retained. This reliably identified the pixels within active neurons in the
296 imaging data and aided in identifying preparations with out-of-plane movement, which
297 were discarded.

298 For baseline activity experiments (Fig 6), the remaining cluster was used as a
299 single ROI and the mean intensity within the ROI was found for each image frame to
300 produce a single time-series for the entire experiment. For visual response experiments
301 (Figs 7-8), pixels within the remaining cluster were automatically divided into groups
302 corresponding to individual L2 terminals using a watershed transform. The mean
303 intensity within each ROI was found for each image frame to produce a single time-
304 series for the entire experiment, and the time-series for all terminal ROIs within an
305 individual animal were then averaged. For Fig 8B-F, ROIs of L2 terminals were first
306 identified automatically, as above, then manually selected individually according to layer
307 position because the 5-HT2B GAL4 SII mutant line labeled other cells in addition to L2
308 neurons.

309 Approximately half of the bath application recordings showed oscillations in
310 activity due to slow, periodic movement of the brain at around 0.04 Hz; we applied a
311 second-order notch filter at this frequency with a bandwidth of 0.005 Hz to remove these
312 oscillations. For the bath application experiments (Fig 6), we plotted $\Delta F/F$, defined as
313 $(F_t-F_0)/F_0$, where F_t is the mean fluorescence in the ROI at the indicated time and F_0 is

314 the mean value of F_t during 60 seconds of baseline activity at the beginning of the
315 experiment and prior to the change in perfusion. For the visual stimulus experiments
316 (Figs 7-8), we again plotted $\Delta F/F$, defined as $(F_t-F_0)/F_0$, where F_t is the mean
317 fluorescence across all individual terminal ROIs at the indicated time and F_0 is the mean
318 of 30 seconds of non-consecutive baseline activity between stimulus presentations
319 during epoch 1 at the beginning of the experiment and prior to the change in perfusion
320 (Fig 7A). For the stimulus response plots (Figs 7B, D, 8C, E), we found the average
321 $\Delta F/F$ time-series within each epoch for each fly after subtracting the average pre-
322 stimulus baseline activity level (0.5 s preceding each flash stimulus) from each time-
323 series, so that all responses started aligned at 0 $\Delta F/F$. For further analysis (Figs 7C, E,
324 8D, F, left), we found the changes in response amplitude across epochs, defined for the
325 dark stimulus presentation (top) as the difference between the pre-stimulus baseline
326 and the maximum $\Delta F/F$ value that occurred up to 1.75 s after cessation of the 0.1 s
327 flash, and for the light stimulus (bottom) as the minimum $\Delta F/F$ value that occurred in the
328 same period of time. For each epoch, we subtracted the value of the responses during
329 epoch 1 at the beginning of the experiment and prior to the change in perfusion, in order
330 to find the change in amplitude relative to epoch 1. We followed a similar procedure for
331 the analysis of peak-peak time (Figs 7C, E, 8D, F, middle), defined as the length of time
332 between the minimum and maximum $\Delta F/F$ values that occurred within 1.75 s after
333 cessation of the 0.1 s flash. The slope of the transient decay was also calculated (Figs
334 7C, E, 8D, F, right). For the visual experiments we examined the baseline changes in
335 fluorescence (Figs 8A-B) after removing responses to the visual stimuli using a series of
336 second-order notch filters at 0.19-0.21 Hz and 0.38-0.42 Hz.

337

338 **Experimental Design and Statistical Tests**

339 Each biological replicate (N) represents one fly, except for RTqPCR and RNA-
340 Seq (Figures 4) where each biological replicate was pooled from 18 or more flies. RT-
341 qPCR experiments include 3 technical replicates, which are averaged to represent a
342 single biological replicate. Animals from at least 3 crosses were used for each
343 experiment. Data for each experiment was collected over 2-6 months in at least 3
344 experiments. No outliers were removed from any data set. Live imaging recordings with
345 too much movement were excluded and not analyzed.

346 For Fig 7 (C, E) and Fig 8 (D, E) comparisons are two-way repeated measure
347 ANOVA (brackets show interactions between time and genotype) and Sidak's multiple
348 comparisons tests, $p \leq 0.05$ *, $p \leq 0.01$**, $p \leq 0.001$***, $p \leq 0.0001$****. These tests were
349 performed using Graphpad Prism Software (San Diego, CA). Differences in baseline
350 calcium shown in Fig 8A-B were calculated by two-tailed Wilcoxon rank sum tests in
351 Matlab R2017a.

352

353

354 **Results**

355 **Serotonin receptors in the optic lobe**

356 Five genes encoding serotonin receptors have been identified in the *Drosophila*
357 genome: 5-HT1A, 5-HT1B, 5-HT2A, 5-HT2B and 5-HT7 (Witz et al., 1990, Saudou et
358 al., 1992, Colas et al., 1995, Gasque et al., 2013, Blenau et al., 2017). To identify
359 specific optic lobe neurons that express each receptor, we expressed the marker
360 mCD8::GFP under the control of a recently characterized panel of T2A-GAL4 insertions
361 in Minos-Mediated Integration Cassettes (MiMICs) located in serotonin receptor gene
362 introns (Gnerer et al., 2015). The GAL4 sequence was inserted into receptor-encoding
363 genes where it acts as an artificial exon and is expected to "mimic" the endogenous
364 gene expression patterns (Venken et al., 2011). Ribosome skipping via T2A allows
365 GAL4 to be expressed as a separate protein, rather than a fusion protein with the
366 serotonin receptor (Diao et al., 2015, Gnerer et al., 2015).

367 We observed distinct expression patterns for each receptor including projections
368 into the neuropils of each of the optic lobe ganglia: the lamina (la), medulla (me), lobula
369 (lo) and lobula plate (lp) (Fig 1A-F). We focus here primarily on receptor subtypes
370 showing expression in the lamina because of the ease of identifying cells based on their
371 morphology (Fischbach and Dittrich, 1989) as well as prominent role of this structure in
372 the earliest stages of visual processing (Joesch et al., 2010, Sanes and Zipursky, 2010,
373 Strother et al., 2014).

374 Receptors 5-HT1A, 5-HT1B and 5-HT2B showed robust labeling of dense
375 projections in the lamina neuropil (Fig 1B, C, E, arrows). Neuronal cell bodies in the
376 lamina cortex are limited to the 5 subtypes of laminar monopolar cells (L1-5) (Fischbach

377 and Dittrich, 1989, Sanes and Zipursky, 2010), and we did not detect GFP expression
378 representing cells expressing either 5-HT1A or 5-HT1B in cell bodies in the lamina
379 cortex (Fig 1B-C). However, we observed somata in the medulla cortex, where cell
380 bodies of neurons that project into both the lamina and medulla—T1, C2, and C3—are
381 located (Fig 1B-C). 5-HT2B driven expression was prominent in the lamina and medulla
382 neuropils (Fig 1E). Additional expression in cell bodies within the lamina cortex,
383 suggested that 5-HT2B might be expressed in one or more subtypes of laminar
384 monopolar cells, since these are the only neuronal cell bodies in this region (Fig 1E).
385 We also observed prominent expression of 5-HT7 in cell bodies within the laminar
386 cortex and extending into the neuropil also consistent with expression in at least one
387 subtype of lamina monopolar cell (Fig 1F). For 5-HT1B and 5-HT2A, additional
388 pleomorphic labeling was observed in the lamina cortex (arrowheads in Fig 1C-D) in a
389 pattern that appeared similar to that of optic lobe glia (Edwards and Meinertzhagen,
390 2010). Based on their location and morphology these cells may be fenestrated or
391 pseudocartridge glia (Edwards and Meinertzhagen, 2010).

392 As shown previously, immunolabeling for serotonin can be observed within the
393 neuropil of all optic ganglia (Fig 1G) (Nässel, 1988, Valles and White, 1988, Sitaraman
394 et al., 2008, Pooryasin and Fiala, 2015, Xu et al., 2016). We also observed a cluster of
395 8-10 cell bodies in the cortical layer of the accessory medulla (Fig 1G-H). These cell
396 bodies correspond to cluster LP2 (or Cb1), previously shown to project into the medulla
397 (Nässel, 1988, Valles and White, 1988, Sitaraman et al., 2008, Pooryasin and Fiala,
398 2015, Xu et al., 2016). Serotonergic boutons in the medulla appeared to be organized in
399 layers corresponding to those that have been previously defined (Fischbach and

400 Dittrich, 1989). This included strong punctate labeling for serotonin at the junction
401 between M1 and M2, as well as additional labeling in M4 and the inner medulla as
402 previously reported (Valles and White, 1988, Monastirioti, 1999, Chang et al., 2006,
403 Pooryasin and Fiala, 2015). Many of the neuronal processes from cells expressing
404 serotonin receptor MiMIC-GAL4 driven GFP showed close apposition to serotonergic
405 boutons. For example, terminals from 5-HT1B-expressing cells in the outer medulla
406 were surrounded by a honeycomb pattern of serotonergic immunolabeling (Fig 1H").

407

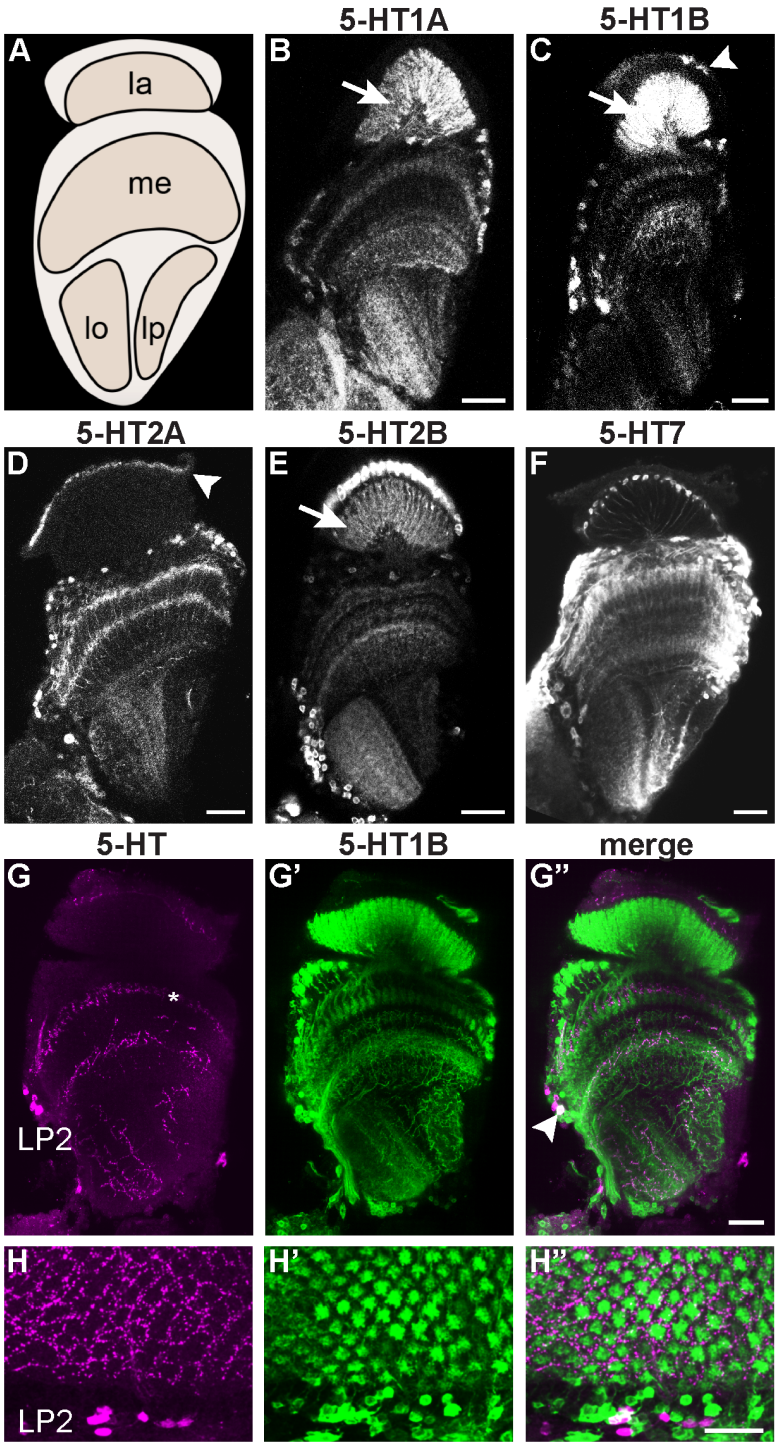

Fig 1. Serotonin receptors and serotonergic projections in the optic lobe. (**A-H**) Serotonin receptor MiMIC-GAL4 lines were crossed to UAS-mCD8::GFP to identify patterns of expression in the optic lobe. (**A**) A schematic of the optic lobe neuropils including the lamina (la), medulla (me), lobula (lo) and lobula plate (lp) with the neuropil in brown and the cortex containing neuronal cell bodies in beige. (**B-F**) GFP-labeled cells representing the 5-HT1A (**B**), 5-HT1B (**C**), 5-HT2A (**D**), 5-HT2B (**E**), and 5-HT7 (**F**). MiMIC-GAL4 lines were visible in all optic lobe neuropils including the lamina neuropil

415 (arrows, B, C, E). The arrowheads in (C, D) mark pleomorphic 5-HT1B and 5-HT2A
416 labeling in the lamina cortex, possibly representing glial expression. (**G**) Anti-serotonin
417 labeled boutons were observed throughout the optic lobe, including medulla layer M2
418 (asterisk) and the indicated LP2 cluster of cells. (**G-G"**). Serotonin receptor
419 5-HT1B>GFP was in proximity to serotonin immunoreactive boutons in M2 and co-
420 labeled at least one serotonergic cell in LP2 (arrowhead). (**H-H"**) In a frontal view,
421 serotonin boutons surround each column containing 5-HT1B>GFP projections in the
422 medulla. n=6-13 brains per condition. Scale bars are 20 μm.

423

424 **Distinct lamina neurons express different serotonin receptors**

425 To identify the cell types that express each serotonin receptor, we used the
426 receptor MiMIC-GAL4 lines described above in combination with the sparse labeling
427 technique MultiColor FlpOut 1 (MCFO) (Nern et al., 2015). Importantly, in contrast to
428 most neurons in the central brain, the stereotyped position and morphology of all
429 neurons in the lamina as well as their organization into repetitive arrays allow them to
430 be unambiguously identified on the basis on their shape and location alone. Although
431 MCFO can be used for lineage tracing (Nern et al., 2015), we induced MCFO in adult
432 flies, when visual system neurons are post-mitotic, and under these conditions MCFO
433 labeling does not represent clonal events. Using 5-HT1A and 5-HT1B MiMIC-GAL4
434 lines with MCFO we observed a subtype of cells with a soma in the medulla cortex, a
435 long basket-like projection in the lamina, and a smaller projection in the medulla (Fig
436 2A-B). This morphology is identical to that of T1 cells and distinct from other cell types
437 in the lamina (Fig 2C) (Fischbach and Dittrich, 1989). T1 cells were identified in 23 of 31
438 brains (71%) for 5-HT1A and in 10 of 11 brains (91%) for 5-HT1B. On average, we
439 observed thirteen MCFO-labeled T1 cells per individual optic lobe for 5-HT1A and nine
440 T1 cells per optic lobe for 5-HT1B. We also found that 5-HT1A>MCFO labeled lamina

441 wide-field neurons (Lawf) in 14 of 31 brains (Fig 2D). In some cases, the proximity of
442 other 5-HT1A+ processes made it difficult to determine the precise number of Lawf
443 neurons per brain. It also remains unclear whether labeled cells represent Lawf1
444 (Fischbach and Dittrich, 1989) (shown in Fig 2C) or Lawf2, which was identified more
445 recently and is not shown in 2C (Hasegawa et al., 2011, Tuthill et al., 2013).

446 Using the 5-HT2B MiMIC-GAL4 driver with MCFO, we observed labeled cells
447 with a soma in the lamina cortex, dense projections extending into the lamina neuropil,
448 and a single bushy terminal in the medulla (Fig 2E), a morphology identical to lamina
449 monopolar neuron L2 and no other laminar cell types (Fig 2C) (Fischbach and Dittrich,
450 1989). We observed L2 cells in 9 of 9 (100%) 5-HT2B>MCFO brains, observing an
451 average of eleven L2 neurons per optic lobe.

452 For 5-HT7>MCFO, we observed lamina monopolar cells in 7 of 13 brains (54%)
453 (Fig 2F), with an average of 20 cells per optic lobe. All of the lamina monopolar cells
454 labeled with 5-HT7>MCFO lacked the dense processes in the neuropil that are
455 characteristic of L1-L3, and also lacked the vertically oriented collaterals in the inner
456 (proximal) lamina seen in L4 neurons (Fig 2C, F). We therefore suggest that 5-HT7 is
457 expressed in the one remaining subtype, L5 cells. Consistent with our observations
458 using 5-HT2A MiMIC-GAL4>GFP, all (18/18, 100%) 5-HT2A>MFCO brains labeled cells
459 with a morphology and location possibly consistent with the fenestrated or
460 pseudocartridge glia in the lamina cortex (Fig 2G) (Edwards and Meinertzhagen, 2010).

461 As noted above, in some cases, multiple cells of each subtype were labeled in
462 each brain. However, we also detected less frequent events for other columnar cells in
463 the lamina. These include observations of multiple centrifugal C2 cells in 3 of 31

464 5-HT1A>MCFO brains (Fig 2H). We also observed a single cell we putatively identify as
465 L2 in one 5-HT7>MCFO brain, compared to 152 presumptive L5 cells counted in the
466 thirteen 5-HT7>MCFO brains. Similarly, we observed 5 lamina monopolar cells labeled
467 with 5-HT2A>MCFO in only 4 brains, compared to hundreds of presumptive glia labeled
468 in all 18 brains (see Fig 2G). We did not detect any examples of serotonin receptor
469 expression in photoreceptors or L3 neurons.

470

471 **Medulla neurons express serotonin receptors**

472 In addition to the 6 subtypes of columnar neurons that express serotonin
473 receptors and extend projections into the lamina (Fischbach and Dittrich, 1989), we
474 have tentatively identified several cells with projections that are either confined to the
475 medulla, or include both medulla and lobula complex and may also express serotonin
476 receptors. Although further work will be needed for more precise identification, their
477 morphology strongly suggest that they represent subtypes of distal medulla (Dm)
478 amacrine neurons, medulla intrinsic (Mi) neurons, and transmedullary Y neurons (TmY).
479 Dm neurons have cell bodies in the medulla cortex but, unlike other medullar neurons,
480 project into the distal medulla (Fischbach and Dittrich, 1989). For 5-HT1B, we observed
481 a single Dm-like cell (Fig 2I). Using 5-HT7>MCFO we observed medulla intrinsic cells,
482 which are confined to the medulla, that are morphologically similar to Mi1 labeled in 6 of
483 13 brains (Fig 2J). TmY cell bodies are located in the medulla cortex and send
484 projections through the medulla; their processes terminate in both the lobula and lobula
485 plate, thus uniquely identifying this cell class (Fischbach and Dittrich, 1989). We
486 observed potential TmY3 cells labeled in five 5-HT1A>MCFO brains (Fig 2K) and four

487 5-HT7>MCFO brains (Fig 2L). We observed TmY cells labeled in all 18 5-HT2A>MCFO
488 brains, with an average of 18 TmY cells per optic lobe (Fig 2M). We anticipate that
489 these data may be useful for comparisons with genomic studies of the optic lobe (Davis
490 et al., 2020) and help to generate hypotheses about the potential serotonergic
491 regulation of these cells.

492

493

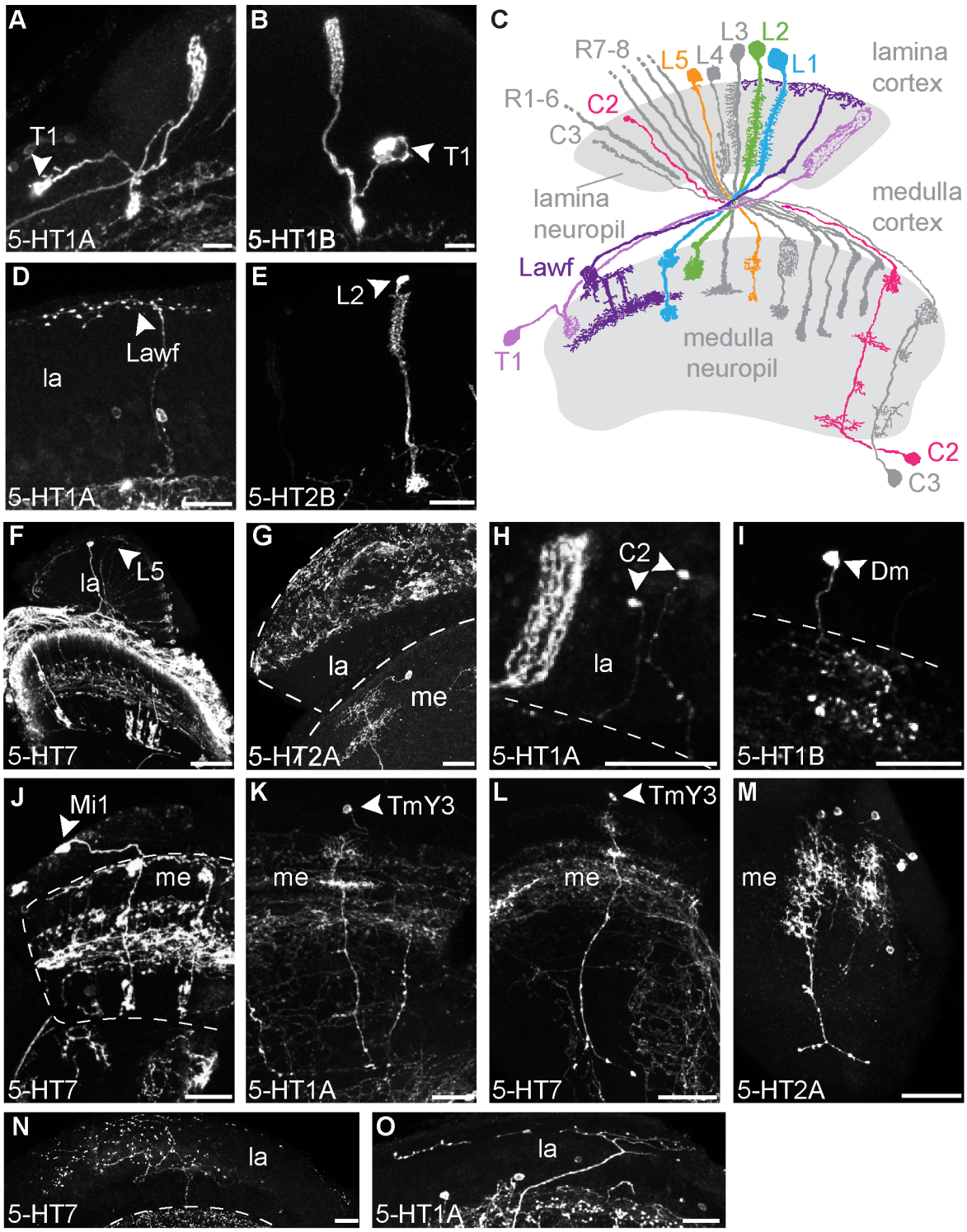

Fig 2. Lamina neurons including T1 and L2 express serotonin receptors. (**A-B, D-O**) Serotonin receptor MiMIC-GAL4 lines were crossed to UAS-MCFO-1 to sparsely label individual cells in the lamina. Cells are indicated by an arrowhead. 5-HT1A (**A,**) and 5-HT1B (**B**) MCFO crosses revealed cells with morphologies identical to T1 neurons. (**C**) A diagram showing lamina neurons adapted from (Fischbach and Dittrich, 1989) highlights L1 (blue), L2 (green), L5 (orange), T1 (purple), C2 (pink), and Lawf (dark purple) cells. (**D**) 5-HT1A>MCFO also labeled Lawf-like cells. (**E**) 5-HT2B>MCFO

501 labeled cells are morphologically identical to L2 neurons. (**F**) 5-HT7>MCFO-1 labeled
502 neurons most likely representing L5 lamina monopolar cells. (**G**) 5-HT2A>MCFO-1 cells
503 in the lamina cortex with a location and morphology consistent with glia. (**H**)
504 5-HT1A>MCFO labeled cells with morphology similar to C2 cells. (**I**) 5-HT1B>MCFO
505 labeled a distal medulla neuron (Dm). (**J**) 5-HT7>MCFO a medulla intrinsic neuron that
506 resembled Mi1. (**K-M**) 5-HT1A, 5-HT7 and 5-HT2A>MCFO labeled TmY cells. (**N-O**)
507 Cells projecting into the lamina cortex were labeled by 5-HT7>MCFO (**N**) and
508 5-HT1A>MCFO (**O**). Scale bars are 20 µm and n=10-31 brains imaged per receptor
509 subtype. Cell types shown were observed in a subset of brains: 22/31 (**A**), 10/11 (**B**),
510 14/31, 14/31 (**D**), 10/10 (**E**), 7/13 (**F**), 18/18 (**G**), 3/31 (**H**), 1/11 (**I**), 7/13 (**J**), 5/31 (**K**),
511 4/13 (**L**), 18/18 (**M**), 3/13 (**N**), and 6/31 (**O**).

512

513 **Serotonin autoreceptors in the optic lobe**

514 In addition to columnar cells, 5HTR>MCFOs labeled several central brain
515 projection neurons that innervate the optic lobe. We observed both 5-HT1A>MCFO and
516 5-HT7>MCFO processes in the lamina cortex and immediately adjacent regions of the
517 neuropil (Fig 2 N-O). In a subset of brains, these co-labeled for anti-serotonin staining
518 (Fig 3A-B) suggesting that these represent serotonergic neurons previously shown to
519 send long range projections into the lamina from the accessory medulla and/or central
520 brain (Valles and White, 1988, Monastirioti, 1999, Chang et al., 2006, Pooryasin and
521 Fiala, 2015). In addition, some processes labeled by 5-HT1B >MCFO co-labeled with
522 serotonin immunolabeled boutons in the inner medulla (iM), medulla layer 4 (M4), and
523 lobula (lo) (Fig 3C). We speculate that these processes are serotonergic and expresses
524 5-HT1B as an autoreceptor, consistent with the fact that 5-HT1B>GFP co-labeled with
525 serotonin-immunoreactive cells in serotonergic cluster LP2 (arrowhead in Fig 1G). We
526 also observed 5-HT7>MCFO projections that co-label with serotonin boutons in the
527 lobula, lobula plate (lp), iM and M4 (Fig 3D). Although we did not comprehensively map
528 all putative serotonin autoreceptors in the central brain, we observed co-localization of
529 5-HT1A and 5-HT1B-MIMIC>GFP with several anti-serotonin immunolabeled cell bodies

530 shown in Fig 1G-G”and Fig 3E-F. Using serotonin cell mapping described in (Nässel,
531 1988, Valles and White, 1988, Sitaraman et al., 2008, Pooryasin and Fiala, 2015) we
532 identified 5-HT1A+ serotonergic clusters as PLP (LP1), SEL, AMP and PMP (Fig 3E.
533 The 5-HT1B+ cell clusters were identified as LP2 (Cb1), PLP (LP1), and PMP, (Fig 1G-
534 G”, arrowhead and Fig 3F). While we have not pursued functional studies of presynaptic
535 serotonergic neurons in this report, the integration of imaging studies in both
536 serotonergic neurons and post-synaptic neurons represents a future goal to assess the
537 interplay between auto- and post-synaptic receptors in visual circuits.

538

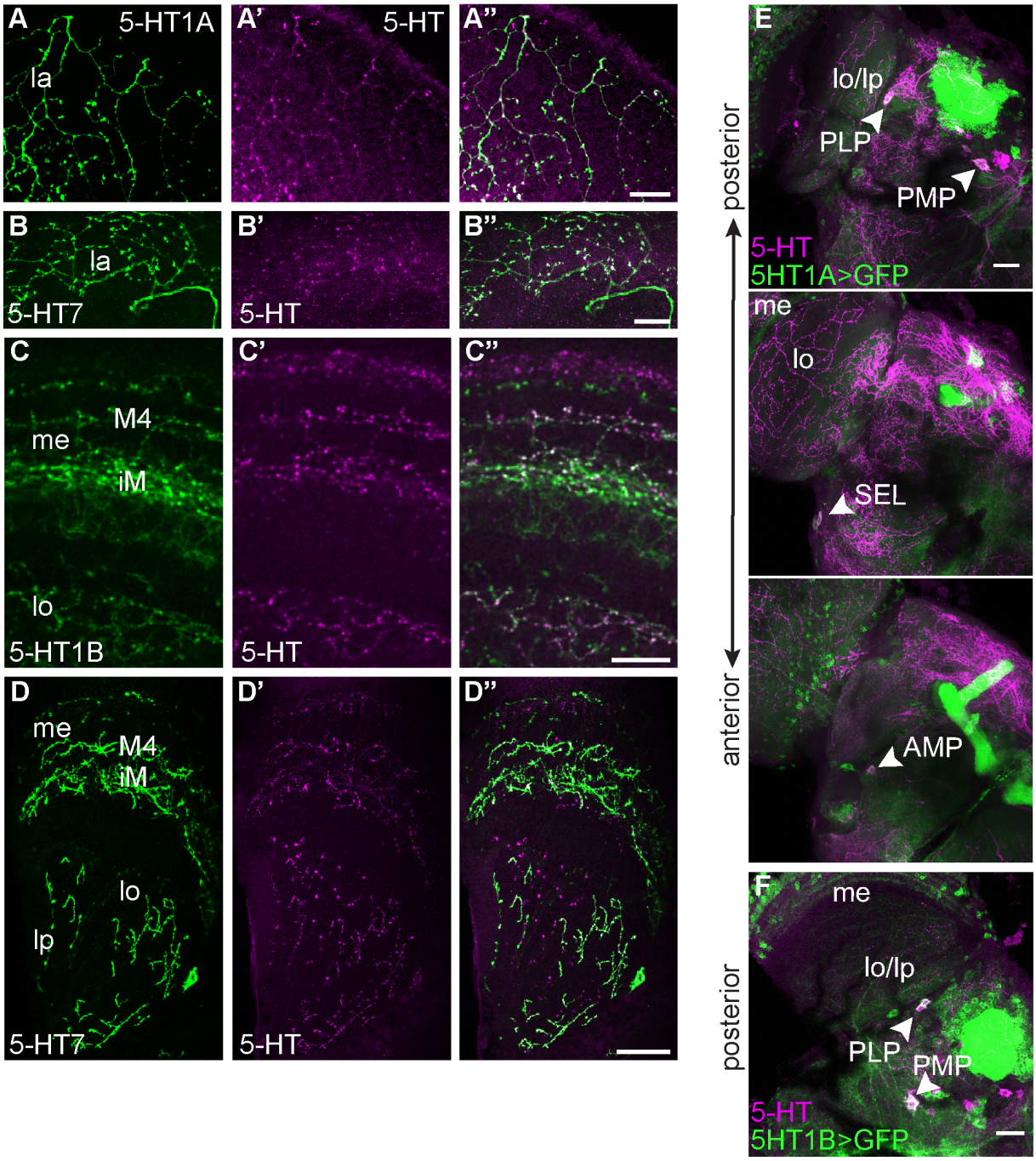

Fig 3. Serotonin Autoreceptors are expressed throughout the Optic Lobe. (**A-D**) Serotonin receptor MiMIC-GAL4 lines were crossed to UAS-MCFO-1 to label individual cells. Anti-serotonin immunohistochemistry was used to identify serotonergic cells. (**A**) A 5-HT1A>MCFO labeled central brain neuron innervates the lamina cortex and the most distal area of the laminar neuropil and co-labeled with anti-serotonin. (**B**) Similarly, a 5-HT7>MCFO labeled projection into the lamina co-labeled with anti-serotonin. (**C**) 5-HT1B>MCFO labeled processes in the inner medulla (iM), medulla layer 4 (M4), and lobula (lo) co-labeled with serotonin immunogenic boutons. (**D**) 5-HT7>MCFO

547 processes co-labeled with anti-serotonin in the iM, M4, lo, and lobula plate (lp). (**E-F**)
548 Serotonin receptor MiMIC-GAL4 driving UAS-mCD8::GFP were co-stained with anti-
549 serotonin immunolabeling to map serotonin autoreceptors to specific cell clusters. **(E)**
550 Anterior to posterior images taken in the same brain show several serotonergic cell
551 clusters expressing 5-HT1A (labeled at arrowheads). (**F**) PLP and PMP serotonin-
552 immunoreactive cells co-label with 5-HT1B>GFP (arrowheads) in the posterior central
553 brain. Scale bars are 20 µm and n=10-31 brains imaged per receptor subtype. Co-
554 localization with anti-serotonin was observed in n=3 (A-B), n=6 (C), n=5 (D), n=12 (**E**),
555 and n=6 (**F**).

556

557 **L2 neurons express 5-HT2B and T1 neurons express 5-HT1A and 5HT1B**

558 A comprehensive genomic study of the optic lobe neurons was recently reported
559 (Davis et al., 2020). Before embarking on further functional studies of specific neurons
560 in the lamina, we sought to confirm the expression of serotonin receptors independently
561 of both (Davis et al., 2020) and the data we obtained using MiMIC GAL4 lines. To this
562 end, we used a separate set of split-GAL4 drivers previously shown to be specific for
563 particular cell types (Tuthill et al., 2013) and focused on a small subset of laminar
564 neurons: T1, L1 and L2. Drivers representing each cell were used to express GFP, and
565 the GFP-labeled cells were isolated via Fluorescence Activated Cell Sorting (FACS).
566 RNA was then extracted from T1, L1 and L2 FACS isolates as well as the unlabeled
567 cells. To probe for serotonin receptor expression in each cell type, we used both RT-
568 qPCR and RNA-Seq. Consistent with our MCFO data, RT-qPCR from GFP-labeled T1
569 isolates (n=6) showed enrichment of both 5-HT1A and 5-HT1B transcripts, but no other
570 serotonin receptors (Fig 4A). Using RNA-Seq, we compared the relative abundance for
571 each receptor by calculating Transcripts Per Million (TPMs). We found that 5-HT1A
572 (182±43 TPM±stdev) and 5-HT1B (278±25 TPM±stdev) were more abundant than other

573 serotonin receptors (range 0.1±0.1 to 2.5±4 TPM±stdev) in T1 samples (n=3, Fig 4B).
574 Using RT-qPCR, L2 isolates showed consistent enrichment for 5-HT2B, but not 5-HT1A
575 or 5-HT1B transcripts (Fig 4C) and higher TPMs for 5-HT2B (130±75 TPM±stdev)
576 compared to other serotonin receptors (range 6±6 to 31±9 TPM±stdev) (Fig 4D). In
577 addition, 5-HT7 was amplified by RT-qPCR in 3/5 L2 samples and 5-HT2A in 1/5 L2
578 samples (Fig 4C). These data are consistent with our MCFO results in which a single L2
579 neuron was identifiable in two 5-HT2A>MCFO brains (2 of 18, 11%) and in one
580 5-HT7>MCFO brain (1 of 13, 8%). By contrast, using RNAseq we did not detect high
581 abundance of either 5-HT2A or 5-HT7 transcripts in L2 neuron isolates. Together, these
582 data suggest that 5-HT2B is most prevalent in L2 cells, but 5-HT7 and 5-HT2A may also
583 be present at low levels or within a subset of L2 cells.

584 We did not observe evidence of any serotonin receptor expression in L1 neurons
585 using the serotonin receptor MiMIC-GAL4 lines to drive either mCD8::GFP (see Fig 1)
586 or MCFO. In agreement with this observation, RT-qPCR from isolated L1 cells showed
587 virtually no receptor expression, apart from one sample weakly enriched for 5-HT1B
588 (Fig 4E). In sum, MCFO sparse labeling in combination with RT-qPCR and RNA-Seq
589 showed that T1 neurons express 5-HT1A and 5-HT1B, and L2 neurons express
590 5-HT2B, whereas L1 neurons do not express any serotonin receptor subtypes that are
591 detectable using these methods.

592 Our data complement a recent transcriptomic analysis (Davis et al., 2020), which
593 reported a high probability of expression for 5-HT2B in L2, 5-HT1A and 5-HT1B in T1,
594 and a low likelihood of any serotonin receptor expression in L1 neurons (Davis et al.,
595 2020). This study did not report a high probability of either 5-HT2A or 5-HT7 expression

596 in L2 neurons, consistent with our observation that 5-HT7 and 5-HT2A may be present

597 either at low levels or within a subset of cells.

598

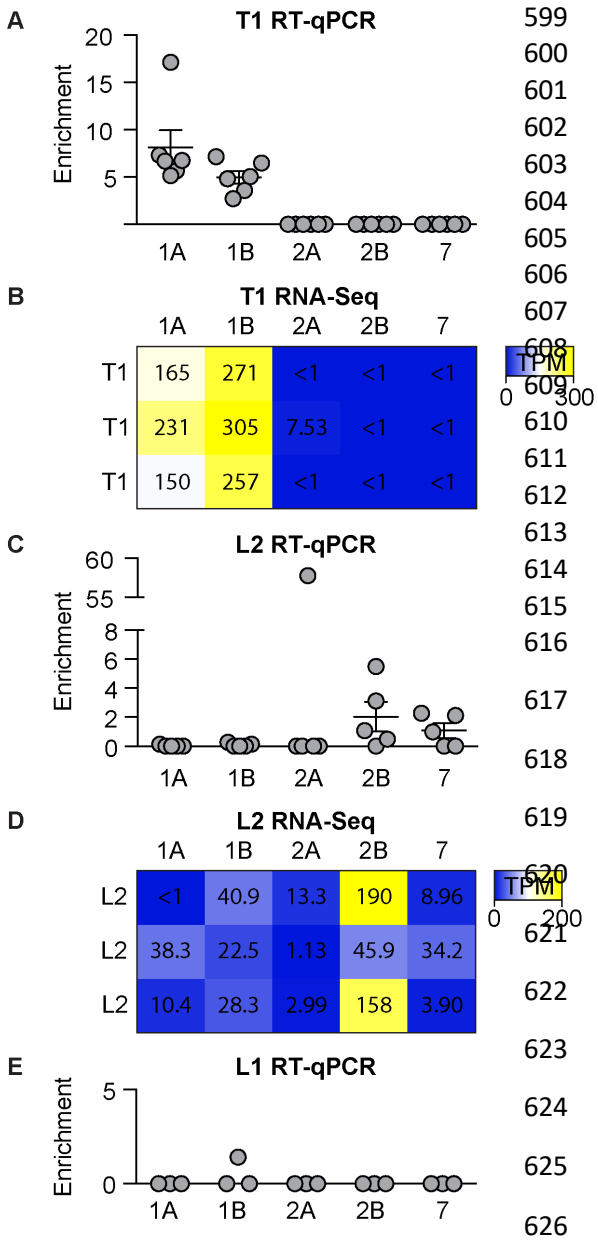

599 **Fig 4. L2 neurons express 5-HT2B and T1**
600 **neurons express both 5-HT1A and**
601 **5-HT1B serotonin receptors.** RT-qPCR
602 performed on cDNA from isolated T1 (**A**) or
603 L2 (**C**) neurons expressing GFP showed
604 enrichment for serotonin receptors relative to
605 other GFP-negative cells from the optic lobe.
606 (**B**) T1 RNA-Seq transcript abundance (color
607 low to high, blue to yellow) Transcripts Per
608 Kilobase Million (TPMs) revealed enriched
609 5-HT1A and 5-HT1B compared to other
610 serotonin receptors. (**D**) L2 RNA-Seq
611 showed higher 5-HT2B TPMs in two of three
612 samples. (**E**) L1 RT-qPCR enrichment for
613 serotonin receptors. RT-qPCR error bars
614 represent mean±SEM. n=3-6 biological
615 replicates pooled from 18-40 brains per
616 replicate.

617

618

619

620

621

622

623

624

625

626

627

628

629 **5-HT2B and 5-HT1A receptors localize to M2**

630 Both T1 and L2 neurons have dense projections in the lamina neuropil and
631 arborize in layer 2 of the medulla neuropil (M2). Serotonin neurons directly innervate M1
632 and M2 of the medulla neuropil raising the possibility that serotonergic signaling might
633 occur at the nerve terminals of T1 and L2 within layer M2. If so, we reasoned that the
634 serotonin receptors expressed in L2 and T1 might localize to M2. To test this possibility,
635 we took advantage of a 5-HT1A allele that had been tagged at the C-terminus with GFP
636 (Deng et al., 2019). The tag was inserted into the endogenous 5-HT1A gene, such that,
637 similar to MiMIC lines (Venken et al., 2011, Gnerer et al., 2015), the receptor-GFP
638 fusion protein is putatively expressed at the same level and in the same cells as the
639 endogenous receptor protein (Deng et al., 2019). In 5-HT1A::GFP flies, we observed
640 enrichment of the tagged protein in layer M2 of the medulla relative to other subcellular
641 sites (Fig 5A-A"). We also observed anti-serotonin immunoreactive boutons that co-
642 labeled with 5-HT1A::GFP in this region (Fig 5B, arrows), suggesting that 5-HT1A may
643 act as both an autoreceptor in serotonergic projection neurons innervating M2 and as a
644 heteroreceptor in columnar neurons that terminate in M2.

645 Since we were unable to obtain an endogenously tagged allele of 5-HT2B, we
646 relied on expression of a UAS-5-HT2B::GFP transgene (Qian et al., 2017) under the
647 control of L2 split-GAL4 to investigate its subcellular localization (Fig 5C). 5-HT2B::GFP
648 was enriched in terminals within M2 of the medulla as compared to the lamina neuropil
649 (Fig 5C-C") and showed additional punctate labeling in L2 cell bodies (Fig 5C',
650 arrowhead). As a control, we expressed UAS-mCD8::GFP using the same L2 split-
651 GAL4 driver. In contrast to 5-HT2B::GFP, labeling with 5-HT2B mCD8::GFP was most

652 prominent in the cell body and proximal processes with progressively weaker labeling
653 through the laminar and medulla neuropil and no enrichment in layer M2 (Fig 5D”).
654 These data suggest that both 5-HT2B and 5-HT1A preferentially localize to the
655 terminals of L2 and T1 respectively in the medulla layer M2 rather than the lamina
656 neuropil. Serotonergic boutons also localize to M1/M2 but are not found in the lamina
657 neuropil near the arborizations of either T1 or L2 neurons (see Fig 1G). Although
658 serotonergic boutons are also found in the lamina cortex near the somata of L2 and T1
659 neurons, we are not aware of any evidence in support of direct signaling to neuronal
660 somata in *Drosophila*. We therefore conclude that serotonergic signaling to L2 and T1
661 via 5-HT2B and 5-HT1A most likely occurs in nerve terminals in layer M2 of the
662 medulla, rather than sites in the lamina that function as inputs for photoreceptor cells.
663 However, since other receptors are expressed in both cell types, we cannot rule out the
664 possibility that serotonergic signaling also occurs at other locations, and perhaps via
665 neurohumoral mechanisms rather than release from proximal serotonergic boutons.

666

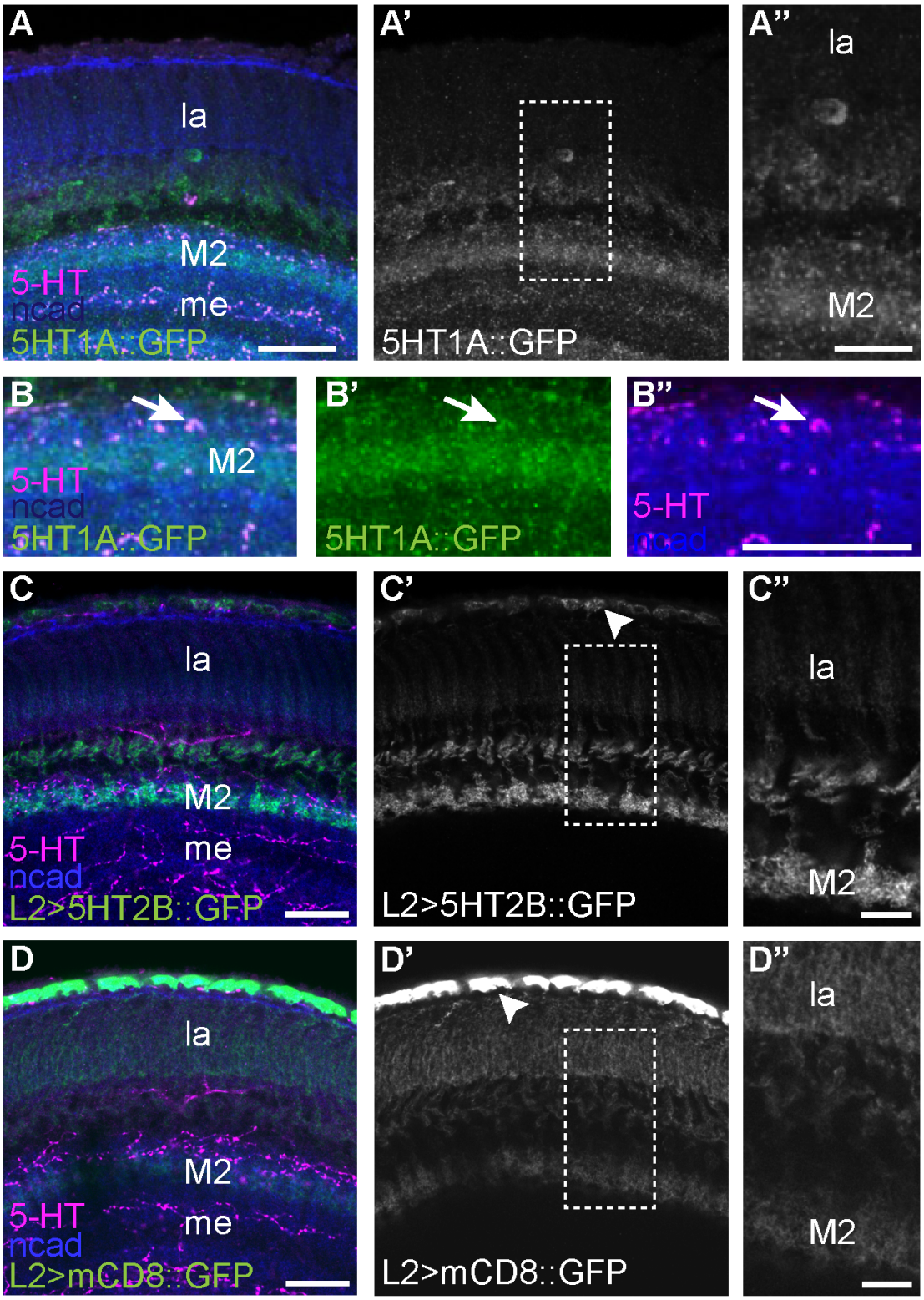
A
la
M2
me
5-HT
ncad
5HT1A::GFP
A'
5HT1A::GFP
A''
la
M2
B
M2
5-HT
ncad
5HT1A::GFP
B'
5HT1A::GFP
B''
5-HT
ncad
C
la
M2
me
5-HT
ncad
L2>5HT2B::GFP
C'
L2>5HT2B::GFP
C''
la
M2
D
la
M2
me
5-HT
ncad
L2>mCD8::GFP
D'
L2>mCD8::GFP
D''
la
M2

667

668

669

670 **Fig 5. Serotonin receptors 5-HT1A and 5-HT2B localize to layer M2 of the medulla.**
671 (**A-A”**) 5-HT1A::GFP localized to layer M2 of the medulla, adjacent to boutons
672 immunogenic for serotonin. Neuropil (N-Cadherin, blue) and serotonin (magenta)
673 labeling provide anatomical context for the lamina (la) and medulla (me). The region
674 specified by the dotted lines in (**A’**) is enlarged in (**A”**). (**B-B”**) In many cases, serotonin
675 immune-reactive boutons co-labeled with 5-HT1A::GFP (arrow). (**C-C”**) Subcellular
676 localization of 5-HT2B was visualized by expressing the fusion construct UAS-5-
677 HT2B::sfGFP in L2 neurons specified by L2split-Gal4. L2>5-HT2B::sfGFP labeling is
678 stronger in the L2 terminals in medulla layer 2 (M2) compared to L2 projections in the
679 lamina (la). Punctate GFP signal is observed in the L2 cell bodies (arrowhead). The
680 region specified by the dotted lines in (**C’**) is enlarged in (**C”**). (**D-D”**) For comparison,
681 membrane-directed UAS-mCD8::GFP was expressed in L2 neurons. L2>mCD8::GFP
682 signal is similar in the medulla and lamina compartments. Strong GFP signal was
683 observed in the cell bodies (arrowhead). The area within the dotted lines in (**D’**) is
684 enlarged in (**D”**). Scale bars are 20 µm in **A-A’**, **B-B”**, **C-C’** and **D-D’**. Scale bars are 10
685 µm in **A”** and 8 µm in **C”** and **D”** Biological replicates are n= for 5-HT1A::GFP (**A-B**),
686 n=15 for L2>5-HT2B::GFP (**C-C”**), and n=10 for L2>mCD8::GFP (**D-D”**).

687

688 **Serotonin increases calcium levels in L2 and L1 neurons**

689 The data presented here and by others (Davis et al., 2020) strongly suggest that
690 L2 cells express serotonin receptors but do not address their functional effects. To
691 address this question, we bath applied serotonin to the optic lobe and used live imaging
692 to monitor cellular activity. The data for receptor expression in L2 was strongest for
693 5-HT2B receptors, which couple with $G_{q/11}$ to increase intracellular calcium *in vitro*
694 (Hoyer et al., 2002, Blenau et al., 2017). We therefore used the genetically encoded
695 calcium indicator GCaMP6f (Chen et al., 2013) to follow changes in L2 activity that
696 might be induced by serotonin. We again employed the L2 split-GAL4 driver (Tuthill et
697 al., 2013) used for transcriptional analysis (Fig 4) to specifically express GCaMP6f in L2
698 neurons (Fig 6A). Since we observed enrichment of 5-HT2B::sfGFP in L2 terminals in
699 M2, we focused our recordings of calcium signaling on these sites. For each
700 experiment, we first recorded a baseline while perfusing the tissue with saline; the

701 perfusion solution was then switched to either saline containing 100 μM serotonin or
702 saline alone. We included tetrodotoxin (TTX) in the perfusion solution to reduce action
703 potential-based inputs to L2 neurons and also to reduce muscle activity driven by action
704 potentials in motor neurons.

705 We consistently observed a large increase in GCaMP6f fluorescence in L2
706 terminals following serotonin application (Fig 6B). This increase continued throughout
707 the time course of recording, peaking at 1.73 ΔF/F ± 0.77 SEM (compared to saline
708 control -0.03 ΔF/F ± 0.05 SEM at the same timepoint; p=0.0095 by two-tailed Wilcoxon
709 rank sum test). Thus, serotonin leads to an accumulation of cytosolic calcium in L2
710 cells, consistent with the predicted outcome of activating $G_{q/11}$ coupled 5-HT2B
711 receptors (Hoyer et al., 2002, Blenau et al., 2017). However, since local neurons in the
712 optic lobe use graded electrical signaling, rather than action potentials, and are
713 insensitive to TTX, we did not block all synaptic inputs to L2 neurons in these
714 experiments, and we cannot rule out cell non-autonomous effects of serotonin on L2
715 neurons.

716

717

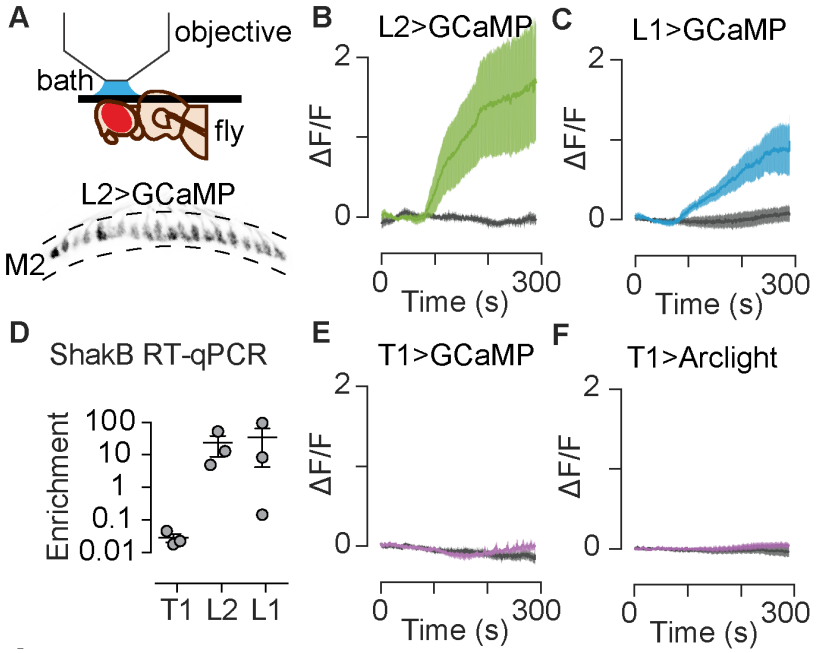

Fig 6. Bath application of serotonin leads to increased calcium in L2 and L1 neurons, but not T1 neurons. (**A-C**) GCaMP6f was paired with L2, L1 and T1 split-GAL4 drivers to monitor responses to 100 μM serotonin (colored traces) or saline controls (gray traces). (**A**) The experimental setup is shown in the top panel, along with a sample image of L2 terminals (bottom panel) as imaged in the medulla (gray). For bath application experiments (**B, C, E, F**), the first 60 s of baseline is not shown; traces represent data recorded following a switch at time 0 to saline with serotonin or saline alone. The length of time for completion of the switch was roughly 100 s. In L2 terminals (**B**), serotonin application led to a significant increase in GCaMP6f signal indicating increased calcium levels as compared to saline controls (p=00095). L1 terminals (**C**) showed a similar increase in calcium following a switch to serotonin (p=0.02). (**D**) RT-qPCR from cell isolates revealed enrichment of the gap junction protein ShakB in L2 and L1, but not T1 neurons. (**E**) T1 cells expressing GCaMP6f showed no significant change in calcium following serotonin application (p>0.05). (**F**) T1 cells expressing the voltage sensor ArcLight similarly displayed no significant change following serotonin application (p>0.05). (**G**) Innexin transcript abundance (Transcripts per Million, TPM) in L2 RNA-Seq samples (n=3). For (**B**, **C**, **E**, **F**) n=4-8 individual flies; the dark trace is an average of all traces and the shaded region is 1 SD; saline vs. serotonin comparisons are two-tailed Wilcoxon rank sum tests. For (**D**), n=3 individual isolates for each cell type. Bars in (**D**) represent the mean±SEM.

741 Since we did not detect serotonin receptors in L1 neurons, we did not expect
742 serotonin to measurably change intracellular calcium levels in these cells. However,
743 with GCaMP6f expressed in L1 cells using a cell-specific driver, we regularly observed a
744 robust increase in baseline fluorescence following serotonin exposure (Fig 6C).
745 Although the increase in GCaMP6f signal did not reach the same response amplitude
746 as observed in L2 neurons, the time course was similar: the signal persisted throughout
747 the recording and peaked at 0.98 ΔF/F ± 0.34 SEM (compared to saline control at 0.07
748 ΔF/F ± 0.09 SEM; p=0.02 by two-tailed Wilcoxon rank sum test). A direct action of
749 serotonin on L1 is unlikely since we did not detect endogenous serotonin receptors (see
750 Figs 1-2, 4). The possibility of action potential driven inputs is also low since TTX was
751 included in the perfusion solution. Other possible mechanisms include graded inputs
752 from neurons unaffected by TTX or coupling between L1 and L2 (Joesch et al., 2010).
753 In support of previous data showing electrical coupling between L1 and L2, we find that
754 transcripts for the gap junction protein Shaking-B (ShakB) are enriched in L1 and L2
755 neurons, but not T1 neurons, using RTqPCR (Fig 6D). In addition, our RNA-Seq data
756 set showed that ShakB (innexin 8) was more abundant in L2 neurons than the other
757 innexins, Inx 1-7, (not shown) consistent with the data of (Davis et al., 2020).

758 We next examined whether serotonin could affect the activity of T1 cells. Both
759 5-HT1A and 5-HT1B receptors, expressed in T1 neurons, are expected to couple with
760 G_i proteins and negatively regulate adenylyl cyclase (Saudou et al., 1992, Hoyer et al.,
761 2002). Due to the generally inhibitory function of these receptors, we hypothesized that
762 serotonin would dampen activity in T1 neurons, possibly manifested as a decrease in
763 cytosolic calcium or membrane potential (Polter and Li, 2010). Using the T1 split-GAL4

764 driver (Tuthill et al., 2013) to express either GCaMP6f or the voltage sensor Arclight
765 (Cao et al., 2013), we did not observe a significant change in fluorescence during
766 perfusion with serotonin (Fig 6E, 6F; p>0.1). Thus, further experiments will be needed to
767 determine the effects of serotonin on T1 neurons. These negative data are nonetheless
768 important for the current study, since the absence of a GCaMP6f response in T1
769 neurons indicates that the response observed in L1 and L2 is not an artifact or a
770 generalized phenomenon common to all cells that extend processes into the lamina.

771

772 **Serotonin in visual processing**

773 To explore the possibility that serotonergic neuromodulation could play a role in
774 visual processing, we next tested whether serotonin would alter the calcium transients
775 in L2 neurons following visual stimulation. We again used GCaMP6f and compared
776 visually induced calcium transients in flies receiving saline or serotonin perfusion. For
777 visual stimulation, we used brief light or dark "flashes" to stimulate L2 neurons as
778 previously described (Yang et al., 2016). Flies were suspended over an LED arena (see
779 Fig 6A) and either a light or dark flash of the entire LED screen (100 ms) was presented
780 at 5 s intervals. Between each flash, the screen showed an intermediate brightness
781 level, indicated as grey in Fig 7A. One-minute epochs consisting of 12 flashes of
782 randomly shuffled polarity were presented six times for each trial (Fig 7A). The first
783 epoch was recorded in saline, followed by a switch to either saline with 100 μM
784 serotonin or saline alone (Fig 7A). During perfusion with either saline or serotonin, dark
785 flashes induced a large increase in calcium that returned to baseline within ~1 second
786 as previously described (Yang et al., 2016) (Fig 7B). The amplitude of the calcium

787 transients following dark flashes increased over the time course of the experiment and
788 there did not appear to be a difference in amplitude in animals receiving serotonin
789 versus saline. However, we detected a modest but statistically significant (p=0.0036 by
790 RM ANOVA) increase in the decay kinetics of the dark flash response in animals
791 perfused with serotonin versus saline alone (Fig 7C) whereby the calcium transient
792 returned to a minimum more quickly with serotonin.

793 In contrast to the response of L2 to dark flashes, light flashes induced a transient
794 stimulus-mediated decrease in GCaMP6f fluorescence, followed by a secondary
795 sustained increase (Fig 7D) as previously reported (Yang et al., 2016). In contrast to
796 dark flashes, we did not observe any significant differences in the amplitude or kinetics
797 of the light flash response in comparing serotonin vs. saline perfusion (Fig 7E). The light
798 flash-evoked drop in fluorescence increased in magnitude over the course of the
799 experiment regardless of whether saline or serotonin was applied (Fig 7E).

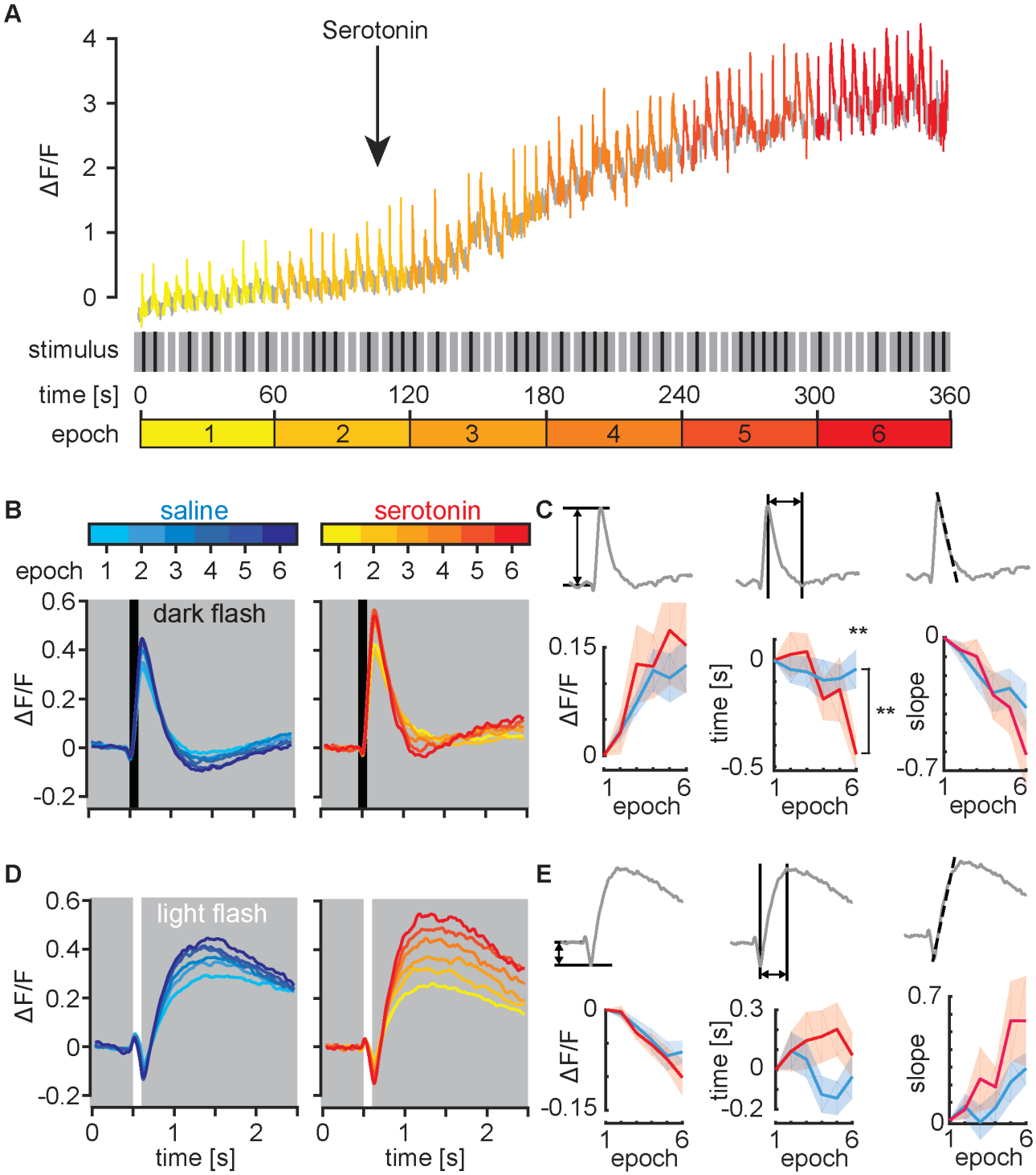
A
Serotonin
ΔF/F
4
3
2
1
0
stimulus
time [s]
0
60
120
180
240
300
360
epoch
1
2
3
4
5
6
B
saline
serotonin
epoch
1 2 3 4 5 6
1 2 3 4 5 6
dark flash
ΔF/F
0.6
0.4
0.2
0
-0.2
C
0.15
0
ΔF/F
time [s]
0
-0.5
**
**
slope
0
-0.7
1
6
epoch
D
light flash
ΔF/F
0.6
0.4
0.2
0
-0.2
0
1
2
time [s]
E
0
-0.15
ΔF/F
0.3
0
-0.2
time [s]
0.7
0
slope

803 **Fig 7**. **Serotonin mediates L2 neuron visually induced calcium transient kinetics**.
804 L2 split GAL4 was crossed to UAS-GCaMP6f to monitor calcium changes following brief
805 light or dark flashes. The preparation was initially perfused with saline alone then and
806 the solution was switched to saline with serotonin or saline control after 1.75 min. A
807 sample experiment with serotonin is shown in (**A**). Light or dark stimuli (middle panel)
808 were flashed at random every 5 s for 6 min, with each min binned into epochs 1-6
809 (lower panel). (**B**) Dark-flashes induced calcium transients for flies receiving saline (left
810 panel, cyan to blue) or serotonin perfusion (right panel, yellow to red). In all animals, L2
811 terminals show a strong increase in GCaMP6f fluorescence following a dark pulse
812 before returning to baseline. (**C**) The time course of each experiment was divided into
813 60 s epochs for analysis and traces representing each progressive 60 s epoch are
814 shown with responses to dark flashes. Dark flash calcium transient amplitude, or
815 maximum ΔF/F, was increased over the course of the experiment for both saline and
816 serotonin-receiving flies (left panel). The time to reach a minimum following the calcium
817 transient was longer in serotonin-perfused tissue compared to saline controls (middle
818 panel), but no change was observed in the transient decay slope (right panel). (**D**)
819 When a light flash was presented in control experiments, L2 cells responded with a
820 decrease in GCaMP signal followed by a large sustained increase. Responses for
821 saline (left panel, cyan to blue) and serotonin perfusion (right panel, yellow to red) are
822 shown. (**E**). The amplitude of the calcium decrease, or minimum ΔF/F, following a light
823 flash was enhanced over the course of the experiment regardless of perfusion solution
824 (left panel). The time to reach a maximum (middle panel) and decay slope were not
825 different in preparations receiving serotonin compared to saline controls. Recordings
826 from individual flies were combined in **B**-**E**, n=14 serotonin and n=20 saline-receiving
827 preparations. Shaded areas show mean +/- SEM. Comparisons are two-way repeated
828 measure ANOVA (brackets show interactions between time and genotype) and Sidak's
829 multiple comparisons tests, p≤0.05 *, p≤0.01**, p≤0.001***, p≤0.0001****.

830

831 Since 5-HT2B is expressed in L2 neurons and is predicted to use calcium as a
832 second messenger we hypothesized that it might mediate the response of L2 neurons
833 to serotonin. We first examined whether loss of 5-HT2B would blunt the gradual
834 increase in baseline calcium we observed in flies exposed to serotonin irrespective of
835 additional light stimuli (Fig 8A). As a negative control for experiments using the 5-HT2B
836 homozygous mutants (-/-) we used heterozygous siblings in which one wild type allele
837 of 5-HT2B was expressed. Similar to wild type flies (Fig 8A), 5-HT2B heterozygous

838 controls perfused with serotonin showed a gradual increase in baseline calcium levels
839 over the six-minute time course of the experiments (Fig 8B). In contrast, in the 5-HT2B -
840 /- mutant, the baseline calcium signal was nearly flat over the time course of the
841 experiment (p=0.0024 by two-tailed Wilcoxon rank sum tests). Although we cannot rule
842 out indirect cell non-autonomous effects from 5-HT2B expression in other cell types, the
843 simplest explanation for the observed results is that activation of 5-HT2B in L2 neurons
844 generates a gradual increase in cytosolic calcium.

845 We next examined whether loss of 5-HT2B would alter the response of L2
846 neurons to light and dark flashes. We hypothesized that loss of 5-HT2B would block
847 changes in the kinetics of the dark-flash calcium response seen with serotonin
848 perfusion. As negative control we again used heterozygous siblings (5-HT2B +/-). As we
849 observed in wild type flies, perfusion of serotonin onto 5-HT2B +/- heterozygous
850 controls led to a gradual reduction in the time required for L2 terminals to reach a
851 minimum after responding to a dark flash (Fig 8D, middle). By contrast, in 5-HT2B -/-
852 homozygous loss of function flies the kinetics of the L2 response to both light and dark
853 flashes remained unchanged over the course of the experiment and continuous
854 perfusion with serotonin (Fig 8D, F). Irrespective of perfusion with saline or serotonin,
855 control flies expressing a functional allele of 5-HT2B showed an increasingly large to
856 response to stimuli over the 6-min experiment (Fig 7C left, 7E left); this increase was
857 not observed in 5-HT2B mutants (Fig 8F left). These data strongly suggest that 5-HT2B
858 mediates the effects of serotonin on the calcium response in L2 neurons, and highlight
859 the importance of using the receptor mutant as a sensitized background to more easily
860 detect the effects of serotonin

861

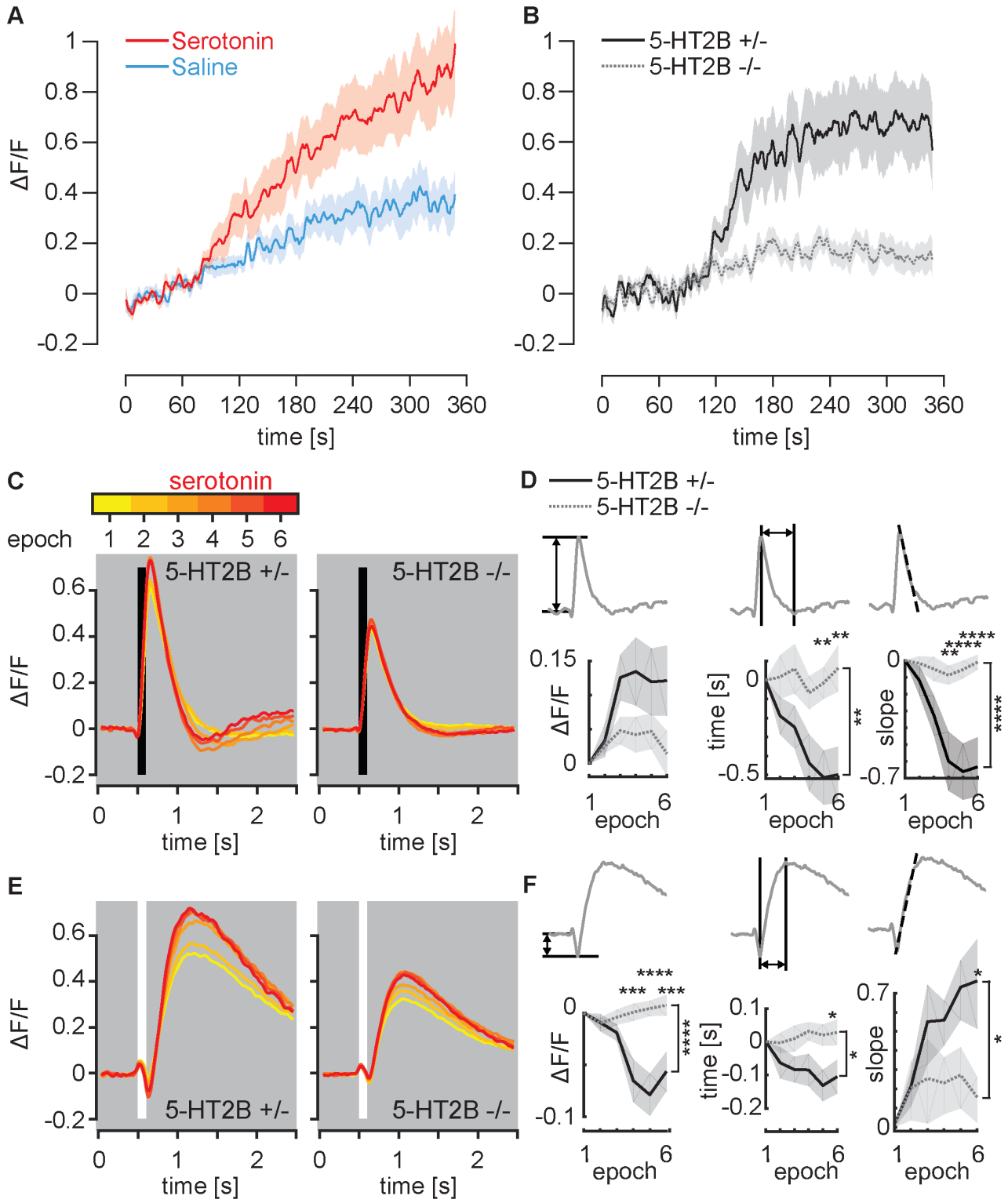

862 **Fig 8. 5-HT2B mediates L2 neuron response serotonin.** (**A**) Serotonin perfusion
863 induced an increase in baseline calcium in 5-HT2B +/+ L2>GCaMP6f lines receiving

serotonin compared to saline controls from Fig 7. (**B**) Mutant 5-HT2B-GAL4 flies were combined with UAS-GCaMP6f to monitor calcium changes in L2 terminals. The serotonin-mediated baseline increase was conserved in 5-HT2B +/- flies, but not present in 5-HT2B -/- flies. (**C**) Dark-flashes induced a strong, transient increase in GCaMP6f fluorescence that returned to baseline in 5-HT2B -/- and 5-HT2B +/- animals receiving serotonin perfusion (**D**) Dark flash calcium transient amplitude, or maximum ΔF/F, was increased over the course of the experiment for 5-HT2B +/- flies, but this was not seen in 5-HT2B -/- flies (left panel). Likewise, the time to reach a minimum following the calcium transient (middle panel) and decay slope (right panel) decreased in 5-HT2B +/- over the experiment but was relatively stable in 5-HT2B -/-. (**E**) When a light flash was presented in control experiments, L2 cells responded with a decrease in GCaMP signal followed by a large sustained increase. Responses for saline (left panel, cyan to blue) and serotonin perfusion (right panel, yellow to red) are shown. (**F**). The amplitude of the hyperpolarization, or minimum ΔF/F, following a light flash was enhanced over the course of the experiment in 5-HT2B +/- flies but remained stable in 5-HT2B -/- flies (left panel). The time to reach a maximum (middle panel) decreased and decay slope (right panel) increased in 5-HT2B +/- flies but both were stable in 5-HT2B -/- flies. For (**A**), n=14 serotonin and n=20 saline preparations were tested. For (**B**-**F**), n=13 5-HT2B +/- and n=15 5-HT2B preparations, all receiving serotonin, were tested. Shaded areas show mean +/- SEM. Comparisons in (**D**, **F**) are two-way repeated measure ANOVA (brackets show interactions between time and genotype) and Sidak's multiple comparisons tests, $p \leq 0.05$ *, $p \leq 0.01$**, $p \leq 0.001$***, $p \leq 0.0001$****.

Discussion

Serotonin modulation occurs by activation of multiple receptors and associated secondary messenger cascades (Nichols and Nichols, 2008, McCorvy and Roth, 2015). Understanding how serotonergic signaling tunes circuit activity requires functional experiments to determine the effects on specific cells as well as mapping the cellular and subcellular cites of individual receptors. To develop the fly visual system as a new molecular genetic model to study serotonergic neuromodulation, we mapped the expression of the five *Drosophila* serotonin receptors in a subset of experimentally tractable cells in the lamina and used live imaging to determine their potential function. To our knowledge, these represent the first functional data for serotonergic neuromodulation of the *Drosophila* visual system with the exception of a single report in

898 1995 (Hevers and Hardie, 1995) and the first data on the subcellular localization of a
899 serotonin receptor in the visual system. In addition, our data mapping the cellular
900 expression pattern of the receptors are complementary to a recently published
901 transcriptomic analysis (Davis et al., 2020) since we have used a completely different
902 experimental approach.

903 To identify cells that express specific receptors and may be amenable to further
904 functional studies we used a combination of MiMIC- based reporter lines, RT-PCR and
905 RNA-Seq. All of these techniques indicate that 5-HT2B is expressed in L2 laminar
906 monopolar neurons, which are involved in motion (Joesch et al., 2010, Takemura et al.,
907 2017b) and contrast vision (Bahl et al., 2015) . Our RT-qPCR results suggest that L2
908 neurons may also express 5-HT7 and 5-HT2A at lower levels or in more restricted
909 subset of cells; however, we did not detect enrichment of these receptors using RNA-
910 Seq. In T1 neurons, we observed consistent expression of 5-HT1A and 5-HT1B (Tuthill
911 et al., 2013). We did not detect any serotonin receptor expression in L1 laminar
912 monopolar neurons, which act in parallel to L2 neurons for visual processing. Our data
913 for L1, L2, T1 neurons are consistent with a recent transcriptional study of the fly visual
914 system (Davis et al., 2020). This study also reported 5-HT1A in C2 and Lawf2 neurons
915 and 5-HT7 in L5 cells, consistent with our sparse labeling experiments (Fig 2). However,
916 unlike Davis et al. we did not detect serotonin receptor expression in photoreceptor cells
917 or in laminar monopolar neuron L3. These discrepancies may result from low or variable
918 levels of expression, which may be biologically important. Further studies may reconcile
919 some of these differences and our data emphasizes the importance of using multiple,
920 overlapping methods to investigate gene expression in complex tissues.

921 Consistent with the predicted coupling of 5-HT2B to G_q, we found that L2
922 neurons respond with a robust increase in calcium measured by GCaMP6f (Fig 6B) and
923 this effect was dramatically reduced in 5-HT2B -/- flies (Fig 8B). The simplest
924 explanation for this result is that 5-HT2B regulates L2 neurons in a cell autonomous
925 manner. However, it remains possible that 5-HT2B expressed in other cells could
926 contribute to this effect. Specific knockdown of 5-HT2B in L2 neurons is required to
927 address this important issue, but available 5-HT2B RNAi lines have been ineffective in
928 our hands. These limitations aside, our data indicate that 5-HT2B can regulate L2
929 neurons, which initiate most of the known visual processing pathways in *Drosophila*.

930 In L1 neurons, which do not express serotonin receptors, we unexpectedly
931 observed a large calcium response to serotonin similar to that of L2 neurons (Fig 6C).
932 These data suggest that L1 cells are indirectly regulated by input from other cells, but
933 further studies will be needed to determine the underlying mechanism. It is possible that
934 the gap junctions that couple L1 and L2 neurons play a role in the indirect serotonergic
935 regulation of L1 (Joesch et al., 2010). Alternatively, inputs from neighboring columnar or
936 wide field neurons that innervate the medulla may be involved. We note that GABAergic
937 C2 neurons (Kolodziejczyk et al., 2008) express 5-HT1A (Fig. 2H also see (Davis et al.,
938 2020)) and are known to synapse onto L1 in M1 (Takemura et al., 2008). Likewise, L5
939 neurons express the 5-HT7 receptor (Fig 2F, also see (Davis et al., 2020)) and
940 reciprocally synapse with L1 neurons in M1 and M5 (Takemura et al., 2008). Since we
941 used TTX to block sodium channel-based action potentials, any inputs to L1 responsible
942 for indirect serotonergic responses are likely to be mediated by graded potentials.
943 These have been well documented in the insect brain including photoreceptor cells and

944 optic lobe neurons (Juusola et al., 1995, Uusitalo et al., 1995, Mu et al., 2012).
945 Regardless of the underlying mechanism, our data on L1 suggest the potential
946 importance of an indirect pathway for serotonergic neuromodulation in this circuit, and
947 the possibility that this may occur in other circuits.

948 In T1 neurons, we were unable to detect any acute change in baseline calcium or
949 voltage in response to serotonin application (Fig 6E-F) and other probes (e.g., for
950 cAMP) may be necessary to detect such a response. However, it is possible that 5-HT1
951 receptors do not induce an acute physiological response, and that more chronic indices
952 are necessary to detect serotonin's effects on T1 neurons.

953 Our observation that molecularly tagged 5-HT2B and 5-HT1A are enriched in the
954 medulla neuropil, underscores the likelihood that the medulla is the most relevant site
955 for serotonergic regulation of these cells. The lamina cortex, which contains the
956 monopolar cell bodies, is also innervated by serotonergic processes. Although we are
957 not aware of any data indicating that neuronal cell bodies receive synaptic input in the
958 fly it is conceivable that serotonin release in the laminar cortex could indirectly regulate
959 neuronal activity, perhaps via glia that may express serotonin receptors (see Fig 1C, 1D
960 and 2G). The potential importance of serotonergic neuromodulation at L2 nerve
961 terminals rather than somatodendritic cites is similar to mechanisms proposed for the
962 mammalian retinogeniculate synapse where 5-HT1 receptors inhibit presynaptic calcium
963 influx (Chen and Regehr, 2003). Similarly, serotonin-induced changes in calcium levels
964 might regulate neurotransmitter release from L2 terminals onto postsynaptic neurons.
965 Investigating this possibility will require the analysis of neurons of downstream of L2.
966 Importantly these neurons may also undergo direct or indirect serotonergic regulation

967 independent of L2 neurons (Takemura et al., 2011, Takemura et al., 2013, Shinomiya et
968 al., 2014). Indeed, (Davis et al., 2020) report serotonin receptors in the neurons that
969 receive input from L1 and L2: Mi1, Tm1, Tm2, and Tm3. Parallel studies in mammals
970 have already begun to dissect the contributions of serotonergic signaling to cells within
971 individual circuits including the visual system (Moreau et al., 2010, Halberstadt, 2015,
972 Gagolewicz and Dringenberg, 2016, Li et al., 2018, Zhou et al., 2018). However, how
973 this information is integrated across circuitry remains poorly understood. The
974 interactions between receptors expressed in L2 and other neurons in the fly visual
975 system provide a new framework to dissect the mechanism by which multiplexed
976 serotonergic inputs combine to regulate circuit function.

977 L1 and L2 neurons receive synaptic input from photoreceptors, and respond to
978 luminance changes with graded potentials, depolarizing in dark conditions and
979 hyperpolarizing in light (Zheng et al., 2006, Clark et al., 2011, Yang et al., 2016). These
980 two neurons feed into pathways for motion and contrast detection (Maisak et al., 2013,
981 Strother et al., 2014, Bahl et al., 2015). The modulation of visually induced calcium
982 transients in L2 following serotonin application (Fig 7-8) suggests a role for serotonin in
983 potentiating the response of L2-dependent visual processing pathways. Our data also
984 suggest a molecular-mechanism for previous observations made in larger insects,
985 including serotonin-induced changes field recordings in blowfly representing the output
986 of L1 and L2 (Chen et al., 1999) and honeybee motion detection in the lobula
987 (Kloppenburg and Erber, 1995) Further examination of the serotonin system in the
988 *Drosophila* optic lobe using the same approaches we employed here can be used to
989 test additional hypotheses related to insect vision.

990 We detected serotonin-mediated differences in the kinetics of L2 neurons'
991 response to visual stimuli in wild type flies, but also measured differences in amplitude
992 when comparing 5-HT2B mutants to heterozygous controls. Without inducible knock-
993 down/out experiments, it is not possible to rule out developmental effects of the 5-HT2B
994 mutant on the L2 neurons. Regardless of possible developmental effects, we
995 emphasize that mutation of 5-HT2B generated a useful sensitized genetic background
996 to uncover effects of serotonin that were not detectable in wild type flies. We speculate
997 that endogenous serotonergic release and activation of 5-HT2B blunted the effects of
998 bath-applied serotonin, making it difficult to detect changes in amplitude due to
999 saturation. A saturation point for neuromodulatory input is critical for circuit stability as
1000 has been described previously (Prinz et al., 2003, Marder, 2011, 2012). In the absence
1001 of 5-HT2B, neither endogenous nor exogenous serotonin would have an effect, thus
1002 increasing our ability to detect the full spectrum of serotonin's actions. More generally
1003 we suggest that our data underscore the power of a genetically sensitized background
1004 to fully understand the mechanisms underlying the aminergic regulation of circuit
1005 function. This approach is well developed in the fly compared to mammalian systems
1006 and we suggest that it can significantly enhance future analyses of serotonergic
1007 neuromodulation.

1008

1009 **Funding:** This work was funded by R01 MH107390 (DEK), R01 MH114017 (DEK) R01
1010 EY026031 (MAF), IOS-1455869 (MAF), R03 DC013997 (AMD), R01 DC016293 (AMD)
1011 and a seed grant from the UCLA Depression Grand Challenge (DEK, MAF). MMS was
1012 supported by a National Science Foundation GRFP, UCLA Cota-Robles fellowship and

1013 F99 NS113454. TRS was supported by a Grant-In-Aid of Research

1014 (G20141015669888) from Sigma Xi, The Scientific Research Society.

1015

1016 **References**

1017 Akin O, Zipursky SL (2016) Frazzled promotes growth cone attachment at the source of
1018 a Netrin gradient in the Drosophila visual system. Elife 5.
1019 Araneda R, Andrade R (1991) 5-Hydroxytryptamine2 and 5-hydroxytryptamine 1A
1020 receptors mediate opposing responses on membrane excitability in rat
1021 association cortex. Neuroscience 40:399-412.
1022 Bahl A, Serbe E, Meier M, Ammer G, Borst A (2015) Neural Mechanisms for Drosophila
1023 Contrast Vision. Neuron 88:1240-1252.
1024 Blenau W, Daniel S, Balfanz S, Thamm M, Baumann A (2017) Dm5-HT2B:
1025 Pharmacological Characterization of the Fifth Serotonin Receptor Subtype of
1026 Drosophila melanogaster. Front Syst Neurosci 11:28.
1027 Borst A, Haag J, Reiff DF (2010) Fly motion vision. Annual review of neuroscience
1028 33:49-70.
1029 Borst A, Helmstaedter M (2015) Common circuit design in fly and mammalian motion
1030 vision. Nature neuroscience 18:1067-1076.
1031 Brunert D, Tsuno Y, Rothermel M, Shipley MT, Wachowiak M (2016) Cell-Type-Specific
1032 Modulation of Sensory Responses in Olfactory Bulb Circuits by Serotonergic
1033 Projections from the Raphe Nuclei. The Journal of neuroscience : the official
1034 journal of the Society for Neuroscience 36:6820-6835.
1035 Cao G, Platisa J, Pieribone VA, Raccuglia D, Kunst M, Nitabach MN (2013) Genetically
1036 targeted optical electrophysiology in intact neural circuits. Cell 154:904-913.
1037 Celada P, Puig MV, Artigas F (2013) Serotonin modulation of cortical neurons and
1038 networks. Frontiers in integrative neuroscience 7:25.
1039 Chang H-Y, Grygoruk A, Brooks ES, Ackerson LC, Maidment NT, Bainton RJ, Krantz
1040 DE (2006) Over-expression of the Drosophila vesicular monoamine transporter
1041 increases motor activity and courtship but decreases the behavioral response to
1042 cocaine. Molecular Psychiatry 11:99-113.
1043 Chen B, Meinertzhagen IA, Shaw SR (1999) Circadian rhythms in light-evoked
1044 responses of the fly's compound eye, and the effects of neuromodulators 5-HT
1045 and the peptide PDF. J Comp Physiol [A] 185:393-404.
1046 Chen C, Regehr WG (2003) Presynaptic modulation of the retinogeniculate synapse.
1047 The Journal of neuroscience : the official journal of the Society for Neuroscience
1048 23:3130-3135.
1049 Chen TW, Wardill TJ, Sun Y, Pulver SR, Renninger SL, Baohan A, Schreiter ER, Kerr
1050 RA, Orger MB, Jayaraman V, Looger LL, Svoboda K, Kim DS (2013)
1051 Ultrasensitive fluorescent proteins for imaging neuronal activity. Nature 499:295-
1052 300.
1053 Cheng KY, Frye MA (2019) Neuromodulation of insect motion vision. J Comp Physiol A
1054 Neuroethol Sens Neural Behav Physiol.
1055 Clark DA, Bursztyn L, Horowitz MA, Schnitzer MJ, Clandinin TR (2011) Defining the
1056 computational structure of the motion detector in Drosophila. Neuron 70:1165-
1057 1177.
1058 Colas JF, Launay JM, Kellermann O, Rosay P, Maroteaux L (1995) Drosophila 5-HT2
1059 serotonin receptor: coexpression with fushi-tarazu during segmentation.

1060 Proceedings of the National Academy of Sciences of the United States of
1061 America 92:5441-5445.
1062 Dacks AM, Christensen TA, Hildebrand JG (2008) Modulation of olfactory information
1063 processing in the antennal lobe of Manduca sexta by serotonin. Journal of
1064 neurophysiology 99:2077-2085.
1065 Davis FP, Nern A, Picard S, Reiser MB, Rubin GM, Eddy SR, Henry GL (2020) A
1066 genetic, genomic, and computational resource for exploring neural circuit
1067 function. Elife 9.
1068 Deng B, Li Q, Liu X, Cao Y, Li B, Qian Y, Xu R, Mao R, Zhou E, Zhang W, Huang J,
1069 Rao Y (2019) Chemoconnectomics: Mapping Chemical Transmission in
1070 Drosophila. Neuron 101:876-893 e874.
1071 Diao F, Ironfield H, Luan H, Shropshire WC, Ewer J, Marr E, Potter CJ, Landgraf M,
1072 White BH (2015) Plug-and-play genetic access to drosophila cell types using
1073 exchangeable exon cassettes. Cell Rep 10:1410-1421.
1074 Dobin A, Davis CA, Schlesinger F, Drenkow J, Zaleski C, Jha S, Batut P, Chaisson M,
1075 Gingeras TR (2013) STAR: ultrafast universal RNA-seq aligner. Bioinformatics
1076 29:15-21.
1077 Edwards TN, Meinertzhagen IA (2010) The functional organisation of glia in the adult
1078 brain of Drosophila and other insects. Progress in neurobiology 90:471-497.
1079 Fischbach KF, Dittrich APM (1989) The optic lobe of Drosophila melanogaster. I. A
1080 Golgi analysis of wild type structure. Cell Tissue Res 258:441-475.
1081 Gagolewicz PJ, Dringenberg HC (2016) Age-Dependent Switch of the Role of
1082 Serotonergic 5-HT1A Receptors in Gating Long-Term Potentiation in Rat Visual
1083 Cortex In Vivo. Neural Plast 2016:6404082.
1084 Gasque G, Conway S, Huang J, Rao Y, Vosshall LB (2013) Small molecule drug
1085 screening in Drosophila identifies the 5HT2A receptor as a feeding modulation
1086 target. Scientific reports 3:srep02120.
1087 Gnerer JP, Venken KJ, Dierick HA (2015) Gene-specific cell labeling using MiMIC
1088 transposons. Nucleic acids research 43:e56.
1089 Halberstadt AL (2015) Recent advances in the neuropsychopharmacology of
1090 serotonergic hallucinogens. Behav Brain Res 277:99-120.
1091 Hasegawa E, Kitada Y, Kaido M, Takayama R, Awasaki T, Tabata T, Sato M (2011)
1092 Concentric zones, cell migration and neuronal circuits in the Drosophila visual
1093 center. Development 138:983-993.
1094 Hevers W, Hardie RC (1995) Serotonin modulates the voltage dependence of delayed
1095 rectifier and Shaker potassium channels in Drosophila photoreceptors. Neuron
1096 14:845-856.
1097 Hoyer D, Hannon JP, Martin GR (2002) Molecular, pharmacological and functional
1098 diversity of 5-HT receptors. Pharmacol Biochem Behav 71:533-554.
1099 Hu Y, Sopko R, Foos M, Kelley C, Flockhart I, Ammeux N, Wang X, Perkins L, Perrimon
1100 N, Mohr SE (2013) FlyPrimerBank: an online database for Drosophila
1101 melanogaster gene expression analysis and knockdown evaluation of RNAi
1102 reagents. G3 (Bethesda) 3:1607-1616.
1103 Joesch M, Schnell B, Raghu SV, Reiff DF, Borst A (2010) ON and OFF pathways in
1104 Drosophila motion vision. Nature 468:300-304.

1105 Juusola M, Uusitalo RO, Weckstrom M (1995) Transfer of graded potentials at the
1106 photoreceptor-interneuron synapse. The Journal of general physiology 105:117-
1107 148.
1108 Keles MF, Frye MA (2017) Object-Detecting Neurons in Drosophila. Current biology :
1109 CB 27:680-687.
1110 Kloppenburg P, Erber J (1995) The modulatory effects of serotonin and octopamine in
1111 the visual system of the honey bee (Apis mellifera L.) II. Electrophysiological
1112 analysis of motion-sensitive neurons in the lobula. J Comp Physiol A Neuroethol
1113 Sens Neural Behav Physiol 176:119-129.
1114 Kolodziejczyk A, Sun X, Meinertzhagen IA, Nassel DR (2008) Glutamate, GABA and
1115 acetylcholine signaling components in the lamina of the Drosophila visual
1116 system. PloS one 3:e2110.
1117 Li YH, Xiang K, Xu X, Zhao X, Li Y, Zheng L, Wang J (2018) Co-activation of both 5-
1118 HT1A and 5-HT7 receptors induced attenuation of glutamatergic synaptic
1119 transmission in the rat visual cortex. Neurosci Lett 686:122-126.
1120 Lombaert N, Hennes M, Gilissen S, Schevenels G, Aerts L, Vanlaer R, Geenen L, Van
1121 Eeckhaut A, Smolders I, Nys J, Arckens L (2018) 5-HTR2A and 5-HTR3A but not
1122 5-HTR1A antagonism impairs the cross-modal reactivation of deprived visual
1123 cortex in adulthood. Mol Brain 11:65.
1124 Lottem E, Lorincz ML, Mainen ZF (2016) Optogenetic Activation of Dorsal Raphe
1125 Serotonin Neurons Rapidly Inhibits Spontaneous But Not Odor-Evoked Activity in
1126 Olfactory Cortex. The Journal of neuroscience : the official journal of the Society
1127 for Neuroscience 36:7-18.
1128 Maisak MS, Haag J, Ammer G, Serbe E, Meier M, Leonhardt A, Schilling T, Bahl A,
1129 Rubin GM, Nern A, Dickson BJ, Reiff DF, Hopp E, Borst A (2013) A directional
1130 tuning map of Drosophila elementary motion detectors. Nature 500:212-216.
1131 Marder E (2011) Variability, compensation, and modulation in neurons and circuits.
1132 Proceedings of the National Academy of Sciences of the United States of
1133 America 108 Suppl 3:15542-15548.
1134 Marder E (2012) Neuromodulation of neuronal circuits: back to the future. Neuron 76:1-
1135 11.
1136 Marder E, O'Leary T, Shruti S (2014) Neuromodulation of circuits with variable
1137 parameters: single neurons and small circuits reveal principles of state-
1138 dependent and robust neuromodulation. Annual review of neuroscience 37:329-
1139 346.
1140 Maroteaux L, Bechade C, Roumier A (2019) Dimers of serotonin receptors: Impact on
1141 ligand affinity and signaling. Biochimie 161:23-33.
1142 McCorvy JD, Roth BL (2015) Structure and function of serotonin G protein-coupled
1143 receptors. Pharmacology & therapeutics 150:129-142.
1144 Meinertzhagen IA, O'Neil SD (1991) Synaptic organization of columnar elements in the
1145 lamina of the wild type in Drosophila melanogaster. The Journal of comparative
1146 neurology 305:232-263.
1147 Monastirioti M (1999) Biogenic amine systems in the fruit fly Drosophila melanogaster.
1148 Microscopy research and technique 45:106-121.

1149 Moreau AW, Amar M, Le Roux N, Morel N, Fossier P (2010) Serotoninergic fine-tuning
1150 of the excitation-inhibition balance in rat visual cortical networks. Cereb Cortex
1151 20:456-467.
1152 Mu L, Ito K, Bacon JP, Strausfeld NJ (2012) Optic glomeruli and their inputs in
1153 Drosophila share an organizational ground pattern with the antennal lobes. The
1154 Journal of neuroscience : the official journal of the Society for Neuroscience
1155 32:6061-6071.
1156 Nadim F, Bucher D (2014) Neuromodulation of neurons and synapses. Current opinion
1157 in neurobiology 29:48-56.
1158 Nässel DR (1988) Serotonin and serotonin-immunoreactive neurons in the nervous
1159 system of insects. Progress in neurobiology 30:1-85.
1160 Nern A, Pfeiffer BD, Rubin GM (2015) Optimized tools for multicolor stochastic labeling
1161 reveal diverse stereotyped cell arrangements in the fly visual system.
1162 Proceedings of the National Academy of Sciences of the United States of
1163 America 112:E2967-2976.
1164 Nichols DE, Nichols CD (2008) Serotonin receptors. Chemical reviews 108:1614-1641.
1165 Petzold GC, Hagiwara A, Murthy VN (2009) Serotonergic modulation of odor input to
1166 the mammalian olfactory bulb. Nature neuroscience 12:784-791.
1167 Picelli S, Bjorklund AK, Faridani OR, Sagasser S, Winberg G, Sandberg R (2013)
1168 Smart-seq2 for sensitive full-length transcriptome profiling in single cells. Nature
1169 methods 10:1096-1098.
1170 Picelli S, Faridani OR, Bjorklund AK, Winberg G, Sagasser S, Sandberg R (2014) Full-
1171 length RNA-seq from single cells using Smart-seq2. Nature protocols 9:171-181.
1172 Polter AM, Li X (2010) 5-HT1A receptor-regulated signal transduction pathways in brain.
1173 Cell Signal 22:1406-1412.
1174 Pooryasin A, Fiala A (2015) Identified Serotonin-Releasing Neurons Induce Behavioral
1175 Quiescence and Suppress Mating in Drosophila. The Journal of neuroscience :
1176 the official journal of the Society for Neuroscience 35:12792-12812.
1177 Prinz AA, Thirumalai V, Marder E (2003) The functional consequences of changes in
1178 the strength and duration of synaptic inputs to oscillatory neurons. The Journal of
1179 neuroscience : the official journal of the Society for Neuroscience 23:943-954.
1180 Pyza E, Meinertzhagen IA (1996) Neurotransmitters regulate rhythmic size changes
1181 amongst cells in the fly's optic lobe. Journal of comparative physiology A,
1182 Sensory, neural, and behavioral physiology 178:33-45.
1183 Qian Y, Cao Y, Deng B, Yang G, Li J, Xu R, Zhang D, Huang J, Rao Y (2017) Sleep
1184 homeostasis regulated by 5HT2b receptor in a small subset of neurons in the
1185 dorsal fan-shaped body of drosophila. Elife 6.
1186 Rivera-Alba M, Vitaladevuni SN, Mishchenko Y, Lu Z, Takemura SY, Scheffer L,
1187 Meinertzhagen IA, Chklovskii DB, de Polavieja GG (2011) Wiring economy and
1188 volume exclusion determine neuronal placement in the Drosophila brain. Current
1189 biology : CB 21:2000-2005.
1190 Sanes JR, Zipursky SL (2010) Design principles of insect and vertebrate visual
1191 systems. Neuron 66:15-36.
1192 Saudou F, Boschert U, Amlaiky N, Plassat JL, Hen R (1992) A family of Drosophila
1193 serotonin receptors with distinct intracellular signalling properties and expression
1194 patterns. The EMBO journal 11:7-17.

1195 Schindelin J, Arganda-Carreras I, Frise E, Kaynig V, Longair M, Pietzsch T, Preibisch S,
1196 Rueden C, Saalfeld S, Schmid B, Tinevez JY, White DJ, Hartenstein V, Eliceiri K,
1197 Tomancak P, Cardona A (2012) Fiji: an open-source platform for biological-
1198 image analysis. Nature methods 9:676-682.
1199 Schmittgen TD, Livak KJ (2008) Analyzing real-time PCR data by the comparative C(T)
1200 method. Nature protocols 3:1101-1108.
1201 Seillier L, Lorenz C, Kawaguchi K, Ott T, Nieder A, Pourriahi P, Nienborg H (2017)
1202 Serotonin Decreases the Gain of Visual Responses in Awake Macaque V1. The
1203 Journal of neuroscience : the official journal of the Society for Neuroscience
1204 37:11390-11405.
1205 Shinomiya K, Huang G, Lu Z, Parag T, Xu CS, Aniceto R, Ansari N, Cheatham N,
1206 Lauchie S, Neace E, Ogundeyi O, Ordish C, Peel D, Shinomiya A, Smith C,
1207 Takemura S, Talebi I, Rivlin PK, Nern A, Scheffer LK, Plaza SM, Meinertzhagen
1208 IA (2019) Comparisons between the ON- and OFF-edge motion pathways in the
1209 Drosophila brain. Elife 8.
1210 Shinomiya K, Karuppudurai T, Lin TY, Lu Z, Lee CH, Meinertzhagen IA (2014)
1211 Candidate neural substrates for off-edge motion detection in Drosophila. Current
1212 biology : CB 24:1062-1070.
1213 Sitaraman D, Zars M, Laferriere H, Chen YC, Sable-Smith A, Kitamoto T, Rottinghaus
1214 GE, Zars T (2008) Serotonin is necessary for place memory in Drosophila.
1215 Proceedings of the National Academy of Sciences of the United States of
1216 America 105:5579-5584.
1217 Strother JA, Nern A, Reiser MB (2014) Direct observation of ON and OFF pathways in
1218 the Drosophila visual system. Current biology : CB 24:976-983.
1219 Takemura SY, Bharioke A, Lu Z, Nern A, Vitaladevuni S, Rivlin PK, Katz WT, Olbris DJ,
1220 Plaza SM, Winston P, Zhao T, Horne JA, Fetter RD, Takemura S, Blazek K,
1221 Chang LA, Ogundeyi O, Saunders MA, Shapiro V, Sigmund C, Rubin GM,
1222 Scheffer LK, Meinertzhagen IA, Chklovskii DB (2013) A visual motion detection
1223 circuit suggested by Drosophila connectomics. Nature 500:175-181.
1224 Takemura SY, Karuppudurai T, Ting CY, Lu Z, Lee CH, Meinertzhagen IA (2011)
1225 Cholinergic circuits integrate neighboring visual signals in a Drosophila motion
1226 detection pathway. Current biology : CB 21:2077-2084.
1227 Takemura SY, Lu Z, Meinertzhagen IA (2008) Synaptic circuits of the Drosophila optic
1228 lobe: the input terminals to the medulla. The Journal of comparative neurology
1229 509:493-513.
1230 Takemura SY, Nern A, Chklovskii DB, Scheffer LK, Rubin GM, Meinertzhagen IA
1231 (2017a) The comprehensive connectome of a neural substrate for 'ON' motion
1232 detection in. Elife 6.
1233 Takemura SY, Nern A, Chklovskii DB, Scheffer LK, Rubin GM, Meinertzhagen IA
1234 (2017b) The comprehensive connectome of a neural substrate for 'ON' motion
1235 detection in Drosophila. Elife 6.
1236 Tan L, Zhang KX, Pecot MY, Nagarkar-Jaiswal S, Lee PT, Takemura SY, McEwen JM,
1237 Nern A, Xu S, Tadros W, Chen Z, Zinn K, Bellen HJ, Morey M, Zipursky SL
1238 (2015) Ig Superfamily Ligand and Receptor Pairs Expressed in Synaptic Partners
1239 in Drosophila. Cell 163:1756-1769.

1240 Trakhtenberg EF, Pita-Thomas W, Fernandez SG, Patel KH, Venugopalan P, Shechter
1241 JM, Morkin MI, Galvao J, Liu X, Dombrowski SM, Goldberg JL (2017) Serotonin
1242 receptor 2C regulates neurite growth and is necessary for normal retinal
1243 processing of visual information. Developmental neurobiology 77:419-437.
1244 Tuthill JC, Nern A, Holtz SL, Rubin GM, Reiser MB (2013) Contributions of the 12
1245 neuron classes in the fly lamina to motion vision. Neuron 79:128-140.
1246 Uusitalo RO, Juusola M, Kouvalainen E, Weckstrom M (1995) Tonic transmitter release
1247 in a graded potential synapse. Journal of neurophysiology 74:470-473.
1248 Valles AM, White K (1988) Serotonin-containing neurons in Drosophila melanogaster:
1249 development and distribution. The Journal of comparative neurology 268:414-
1250 428.
1251 Venken KJ, Schulze KL, Haelterman NA, Pan H, He Y, Evans-Holm M, Carlson JW,
1252 Levis RW, Spradling AC, Hoskins RA, Bellen HJ (2011) MiMIC: a highly versatile
1253 transposon insertion resource for engineering Drosophila melanogaster genes.
1254 Nature methods 8:737-743.
1255 Wilson RI, Turner GC, Laurent G (2004) Transformation of olfactory representations in
1256 the Drosophila antennal lobe. Science 303:366-370.
1257 Witz P, Amlaiky N, Plassat JL, Maroteaux L, Borrelli E, Hen R (1990) Cloning and
1258 characterization of a Drosophila serotonin receptor that activates adenylate
1259 cyclase. Proceedings of the National Academy of Sciences of the United States
1260 of America 87:8940-8944.
1261 Xu L, He J, Kaiser A, Graber N, Schlager L, Ritze Y, Scholz H (2016) A Single Pair of
1262 Serotonergic Neurons Counteracts Serotonergic Inhibition of Ethanol Attraction in
1263 Drosophila. PloS one 11:e0167518.
1264 Yang HH, St-Pierre F, Sun X, Ding X, Lin MZ, Clandinin TR (2016) Subcellular Imaging
1265 of Voltage and Calcium Signals Reveals Neural Processing In Vivo. Cell
1266 166:245-257.
1267 Zheng L, de Polavieja GG, Wolfram V, Asyali MH, Hardie RC, Juusola M (2006)
1268 Feedback network controls photoreceptor output at the layer of first visual
1269 synapses in Drosophila. The Journal of general physiology 127:495-510.
1270 Zhou X, Zhang R, Zhang S, Wu J, Sun X (2018) Activation of 5-HT1A receptors
1271 promotes retinal ganglion cell function by inhibiting the cAMP-PKA pathway to
1272 modulate presynaptic GABA release in chronic glaucoma. The Journal of
1273 neuroscience : the official journal of the Society for Neuroscience.

1274

1275